

General Disclaimer

One or more of the Following Statements may affect this Document

- This document has been reproduced from the best copy furnished by the organizational source. It is being released in the interest of making available as much information as possible.
- This document may contain data, which exceeds the sheet parameters. It was furnished in this condition by the organizational source and is the best copy available.
- This document may contain tone-on-tone or color graphs, charts and/or pictures, which have been reproduced in black and white.
- This document is paginated as submitted by the original source.
- Portions of this document are not fully legible due to the historical nature of some of the material. However, it is the best reproduction available from the original submission.

PSU-IRL-IR-56

Classification Numbers 1.5.1, 3.2.2

~~Report~~

~~NSR~~



THE PENNSYLVANIA
STATE UNIVERSITY

IONOSPHERIC RESEARCH

LOW LATITUDE MIDDLE ATMOSPHERE IONIZATION STUDIES

by

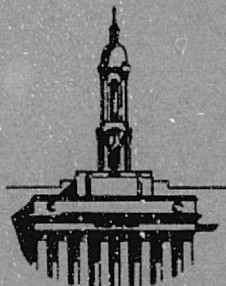
Joseph Peter Bassi

May 1976

*The research reported in this document was partially supported
by The National Aeronautical and Space Administration under
Grant No. NSG-6004.*

NGR-39-009-2/8

IONOSPHERE RESEARCH LABORATORY



University Park, Pennsylvania



N76-22787

Unclas
25283

G3/4b

(NASA-CF-147141) ICW LATITUDE MIDDLE
ATMOSPHERE IONIZATION STUDIES (Pennsylvania
State Univ.) 67 P HC \$4.50 CACL 04A

REPORT DOCUMENTATION PAGE		READ INSTRUCTIONS BEFORE COMPLETING FORM
1. REPORT NUMBER 56	2. GOVT ACCESSION NO.	3. RECIPIENT'S CATALOG NUMBER
4. TITLE (and Subtitle) Low Latitude Middle Atmosphere Ionization Studies		5. TYPE OF REPORT & PERIOD COVERED Internal Report
		5. PERFORMING ORG. REPORT NUMBER PSU-IRL-IR-56
7. AUTHOR(s) Joseph Peter Bassi		8. CONTRACT OR GRANT NUMBER(s) NASA MAP NGL-6004
9. PERFORMING ORGANIZATION NAME AND ADDRESS The Ionosphere Research Laboratory 318 Electrical Engineering East Building University Park, Pennsylvania 16802		10. PROGRAM ELEMENT, PROJECT, TASK AREA & WORK UNIT NUMBERS
11. CONTROLLING OFFICE NAME AND ADDRESS		12. REPORT DATE May 1976
		13. NUMBER OF PAGES 58
14. MONITORING AGENCY NAME & ADDRESS (if different from Controlling Office)		15. SECURITY CLASS. (of this report) NONE
		15a. DECLASSIFICATION/DOWNGRADING SCHEDULE
16. DISTRIBUTION STATEMENT (of this Report)		
17. DISTRIBUTION STATEMENT (of the abstract entered in Block 20, if different from Report) Supporting Agencies		
18. SUPPLEMENTARY NOTES		
19. KEY WORDS (Continue on reverse side if necessary and identify by block number) D-Region Rocket-Satellite Techniques and Measurements		
20. ABSTRACT (Continue on reverse side if necessary and identify by block number) This paper describes a study of low latitude middle atmosphere ionization. With data obtained from three blunt conductivity probes and one Gerdien condenser, all rocket launched and deployed on parachutes during the 1975 "Antarqui" in Peru, an investigation has been conducted into the effects of various ionization sources in the 40 to 65 Km altitude range. A comparison of the two instrument types suggests that they yield consistent results. An observed enhancement of positive ion conductivity taking place during the night can be explained by an		

atmospheric effect, with cosmic rays being the only source of ionization, only if the ion-ion recombination coefficient (α_i) is small ($< 10^{-7} \text{ cm}^3 \text{ s}^{-1}$) and varies greatly with altitude. More generally accepted values of α_i ($\sim 3 \times 10^{-7} \text{ cm}^3 \text{ s}^{-1}$) require an additional source of ionization peaking at about 65 Km, and corresponding approximately to the integrated effect of an X-ray flux measured on a rocket flown in conjunction with the ionization measurements. The physically reasonable assumption of an α_i which does not vary with altitude in the 50-70 Km range implies an even greater value α_i and a more intense and harder X-ray spectrum.

NONE

PSU-IRL-IR-56
Classification Numbers 1.5.1, 3.2.2

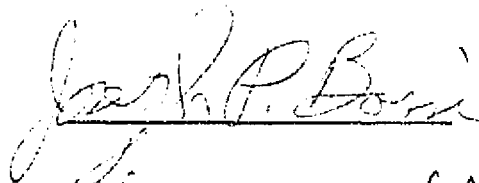
Low Latitude Middle Atmosphere
Ionization Studies

by

Joseph Peter Bassi

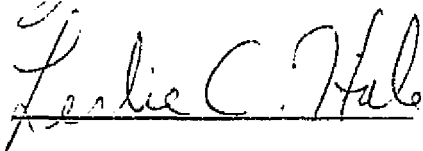
May 1976

The research reported in this document was partially supported by
The National Aeronautical and Space Administration under
Grant No. NSG-6004.



Joseph Peter Bassi

Approved:



Leslie C. Hale

Ionosphere Research Laboratory
The Pennsylvania State University
University Park, Pennsylvania 16802

ACKNOWLEDGEMENTS

The author thanks Dr. L. C. Hale of The Ionosphere Research Laboratory, Department of Electrical Engineering, and Dr. J. J. Olivero for their guidance and encouragement in this research. Also, many discussions with Dr. C. Croskey proved very helpful in this endeavor.

In addition, I appreciate the cooperation of the following in support of this thesis: Air Training Command (ATC), The Air Force Institute of Technology (AU), The Air Weather Service (MAC) of the U.S.A.F., and Major F. Lombardo, USAF. The data contained in this research was obtained on NASA Grant No. NGR 39-009-218.

Finally, I thank Dr. H. A. Panofsky for reading and commenting upon the final draft of this thesis.

TABLE OF CONTENTS

	Page
ACKNOWLEDGEMENTS	ii
LIST OF FIGURES	iv
ABSTRACT	vi
CHAPTER I INTRODUCTION	1
1.1 Middle Atmosphere Ionization.	1
1.2 Importance and Scope of this Research	2
CHAPTER II DESIGN AND DISCUSSION OF INSTRUMENTS	4
2.1 Ion Collection Theory	4
2.2 The Blunt Probe	5
2.3 The Gerdien Condenser	11
2.4 Comparison of Blunt Probe and Gerdien Condenser Measured Conductivities	15
CHAPTER III EXPERIMENTAL RESULTS	18
3.1 Conductivity Profiles	18
3.2 Discussion of Data.	19
3.3 Positive Ion Densities.	24
3.4 Experimental Errors	28
CHAPTER IV THEORETICAL CONSIDERATIONS	30
4.1 Ionization Sources Considered	30
4.2 The Continuity Equation	33
4.3 Solution of the Continuity Equation	33
4.4 Analysis of Calculated Ion Density Versus Time Profiles	34
4.5 A Constant Recombination Coefficient Assumption.	49
CHAPTER V CONCLUSIONS	51
REFERENCES	53
APPENDIX A PROGRAM TO CALCULATE CONDUCTIVITIES	55
APPENDIX B PROGRAM TO CALCULATE N^+ VERSUS TIME CURVES	57

LIST OF FIGURES

Figure		Page
2.1	The Blunt Probe Assembly.	7
2.2	Sweep Voltage and Typical Tele- metered Current	10
2.3	A Simple Gerdien Condenser.	12
2.4	Comparison of Blunt Probe and Gerdien Condenser Measured Positive Conductivities.	16
3.1	Conductivities for 1430 EST, 28 May; 2007 EST, 23 May; and 0200 EST, 24 May, Peru	21
3.2	Composite of σ^+ Profiles for "Antarqui" (Equatorial) and Mid-latitudes.	23
3.3	Gerdien Ion Densities for 1630 EST, 23 May, Peru.	25
3.4	Calculated Ion Densities for 1430 EST, 23 May, Peru.	27
4.1	Production Rates Due to Various Nighttime Ionization Sources.	31
4.2	N^+ Versus Time at 65 Km	36
4.3	N^+ Versus Time at 64 Km	37
4.4	N^+ Versus Time at 63 Km	38
4.5	N^+ Versus Time at 62 Km	39
4.6	N^+ Versus Time at 61 Km	40
4.7	N^+ Versus Time at 60 Km	41
4.8	N^+ Versus Time at 59 Km	42
4.9	N^+ Versus Time at 58 Km	43
4.10	N^+ Versus Time at 57 Km	44
4.11	N^+ Versus Time at 56 Km	45
4.12	N^+ Versus Time at 55 Km	46

Figure		Page
4.13	α_i 's Versus Altitude	47
4.14	Additional Production Needed If Constant α_i is Assumed	50

ABSTRACT

This paper describes a study of low latitude middle atmosphere ionization. With data obtained from three blunt conductivity probes and one Gerdien condenser, all rocket launched and deployed on parachutes during the 1975 "Antarqui" in Peru, an investigation has been conducted into the effects of various ionization sources in the 40 to 65 Km altitude range. A comparison of the two instrument types suggests that they yield consistent results. An observed enhancement of positive ion conductivity taking place during the night can be explained by an atmospheric effect, with cosmic rays being the only source of ionization, only if the ion-ion recombination coefficient (α_i) is small ($<10^{-7} \text{ cm}^3 \text{ s}^{-1}$) and varies greatly with altitude. More generally accepted values of α_i ($\sim 3 \times 10^{-7} \text{ cm}^3 \text{ s}^{-1}$) require an additional source of ionization peaking at about 65 Km, and corresponding approximately to the integrated effect of an X-ray flux measured on a rocket flown in conjunction with the ionization measurements. The physically reasonable assumption of an α_i which does not vary with altitude in the 50-70 Km range implies an even greater value α_i and a more intense and harder X-ray spectrum.

CHAPTER I
INTRODUCTION1.1 Middle Atmosphere Ionization

Our knowledge of the middle atmosphere (30-80 Km altitude range), including the lower ionosphere, is incomplete. This region is characterized by large neutral species density and a weakly ionized plasma, yet the fundamental but complex mechanisms and atmospheric constituents in this region are still only partially understood. Species concentrations and chemical reaction rates, for example, are usually given as approximate values and, in many cases, only order of magnitude estimates. The uncertainty in these atmospheric parameters make it extremely difficult to distinguish the relative importance of various atmospheric processes.

Despite the aforementioned difficulties, some general observations about ionization sources in the lower ionosphere can be made. The ionization of the middle atmosphere is produced by several energetic, therefore deeply penetrating, energy sources. According to accepted views (Whitten and Poppoff, 1969), the most significant ionization sources under undisturbed or "quiet" solar and geophysical conditions is the (Solar) Lyman α (1216 A°) ionization of NO (Nicolet and Aikin, 1960). If disturbed solar conditions exist, the enhanced X-ray flux from the sun becomes important. Finally, at lower altitudes during the day and at all altitudes

at night galactic cosmic rays which will ionize all atmospheric constituents become predominant (Velinov, 1968). The crossover between cosmic ray and Lyman α production is usually at 63.5 Km (Hale, 1973).

Recently, however, a number of investigators suggest that an additional nighttime source of ionization must be considered: galactic X-rays (Ananthakrishnan, 1969; Chilton, 1972). Most of these observations concerned the change of VLF signal phase between two monitoring stations. It was reported that increased electron production rates due to the transit of strong X-ray sources Sco X-1, Tau X-1, and the galactic center produced these observed changes in VLF phase (Sharma, 1972; Mitra, 1972). This matter is still an issue of controversy since other investigators contend the increased electron production due to celestial X-rays is only on the order of a few percent (Poppoff and Whitten, 1969).

Goldberg (1975) has proposed that some X-ray effects may not be due to celestial sources, but Bremsstrahlung produced in the upper ionosphere (F-Region).

1.2 Importance and Scope of This Research

This research will contribute to the knowledge of the middle atmosphere in a number of ways. Firstly, very few studies of this height range have been done at equatorial latitudes. The data employed in this work were obtained during the "Antarqui" D-Region campaign in Peru,

in May of 1975. (This was intended to be an intensive investigation of the constituents and processes of this region.) This research should then contribute appreciably to the understanding of middle atmosphere processes in these latitudes. Further, conductivity and density data were obtained by two different types of direct sensing devices constructed here at The Ionosphere Research Laboratory under the guidance of Dr. L. C. Hale: the Blunt Probe and the Gerdien Condenser, both are rocket launched and parachute borne instruments. This will only be the second time that the conductivity measurements obtained by these two experiments, at low latitudes, will be compared. (Meteorological balloons or electromagnetic wave techniques are not useful in this region.)

Secondly, these data, combined with reasonable assumptions, will be used in solving a simple production-loss (mechanism) continuity equation. Since cosmic ray production is well known (\propto density) and X-ray flux was measured as part of the "Antarqui" campaign, ion density versus time profiles will be constructed and compared to observed ion densities. These are, in turn, proportional to conductivity enhancements. This will enable us to obtain a qualitative and quantitative grasp on, and therefore a better understanding of, some of the processes and ionization sources of the low latitude middle atmosphere.

CHAPTER II

DESIGN AND DISCUSSION OF INSTRUMENTS

2.1 Ion Collection Theory

Both types of instruments used in these studies employ a similar theory of ion collection; this simple theory of positive ion collection will now be briefly discussed.

The fundamental equation for positive ion collection to a probe surface, before the instrument becomes saturated is:

$$J = N^+eS + \mu N^+e \nabla V - eD\nabla N^+ \quad (2.1)$$

where N^+ is the positive ion density, J is the current density; D is the coefficient of diffusion of positive ions; V is potential; e is electrostatic charge; and S is the convection velocity (Farrokh, 1975).

The first term of the right hand side of equation (2.1) is a convection term, the second represents the effect of conduction, and the third term is due to diffusion. If it is assumed that the air flow is parallel to the central axis of the instrument, the convection term can be neglected and equation (2.1) becomes:

$$J = \mu N^+e\nabla V - eD\nabla N^+ \quad (2.2)$$

Also, with the added assumption that ∇N^+ has a value at most the same order of ∇V , the second term of equation (2.2) can be neglected (Farrokh, 1975) and equation (2.2) becomes:

$$J = \mu N^+e\nabla V \quad (2.3)$$

Equation (2.3) is the fundamental relation for a simple mobility charged particle collection mechanism. Hoult (1965) and Sonin (1967) have demonstrated that the equation of the form (2.3) is applicable to a number of different type probe devices and geometries operating in a conductive, continuous medium.

2.2 The Blunt Probe

The bipolar conductivity of a weakly ionized plasma, such as the lower ionosphere in the 30-80 KM altitude range, can be measured by a two electrode, simple mobility mechanism device known as a blunt probe. This instrument was originally designed and constructed by L. C. Hale, D. P. Hoult and associated students of The Ionosphere Research Laboratory in 1964. Since then, it has been used regularly and extensively by this group in studying the "normal" daytime and nighttime D-region. Also, the effects of events such as solar eclipses, "winter anomalies", and polar cap absorptions, upon the lower ionosphere have been investigated with the blunt probe technique (Mitchell, 1973).

Hoult (1965) first described the theory of collecting charged particle species by a subsonic blunt probe under certain specific conditions. These conditions are that; 1) the convective flow must be much greater than diffusion and "ion mobility" until very close to the collecting surface, 2) the space charge density is low enough

that it may be neglected in calculating the electric field in the probe, and 3) the mobility must be definable in a physical sense.

If these conditions are satisfied, ion collection can be expressed by a simple "mobility mechanism" as discussed above:

$$dI = eN\mu EdA$$

where dI is the current collected by the element of probe surface dA , E is the electric field at the surface, μ is the ion mobility and N is the number density of charged particles collected. This equation is analogous to equation (2.3), the general equation describing simple mobility collection theory.

Figure 2.1 is an example of the probe system. An aluminum disk is located at the end of the cylindrical payload housing. The probe disk faces downward, suspended from the parachute, into the flow. The central portion of the disk is used as the collecting electrode. It is held at the same potential as the rest of the disk, which now serves as a guard electrode. The remainder of the payload housing is used as a return electrode (Hale, 1965).

The potential (V_p) of the flat plate charged particle sensor, which consists of a central collecting surface and a concentric guard ring of radius a and R respectively, is varied. The electric field, E is given by:

$$E = (2V_p)/\pi R \quad (2.4)$$

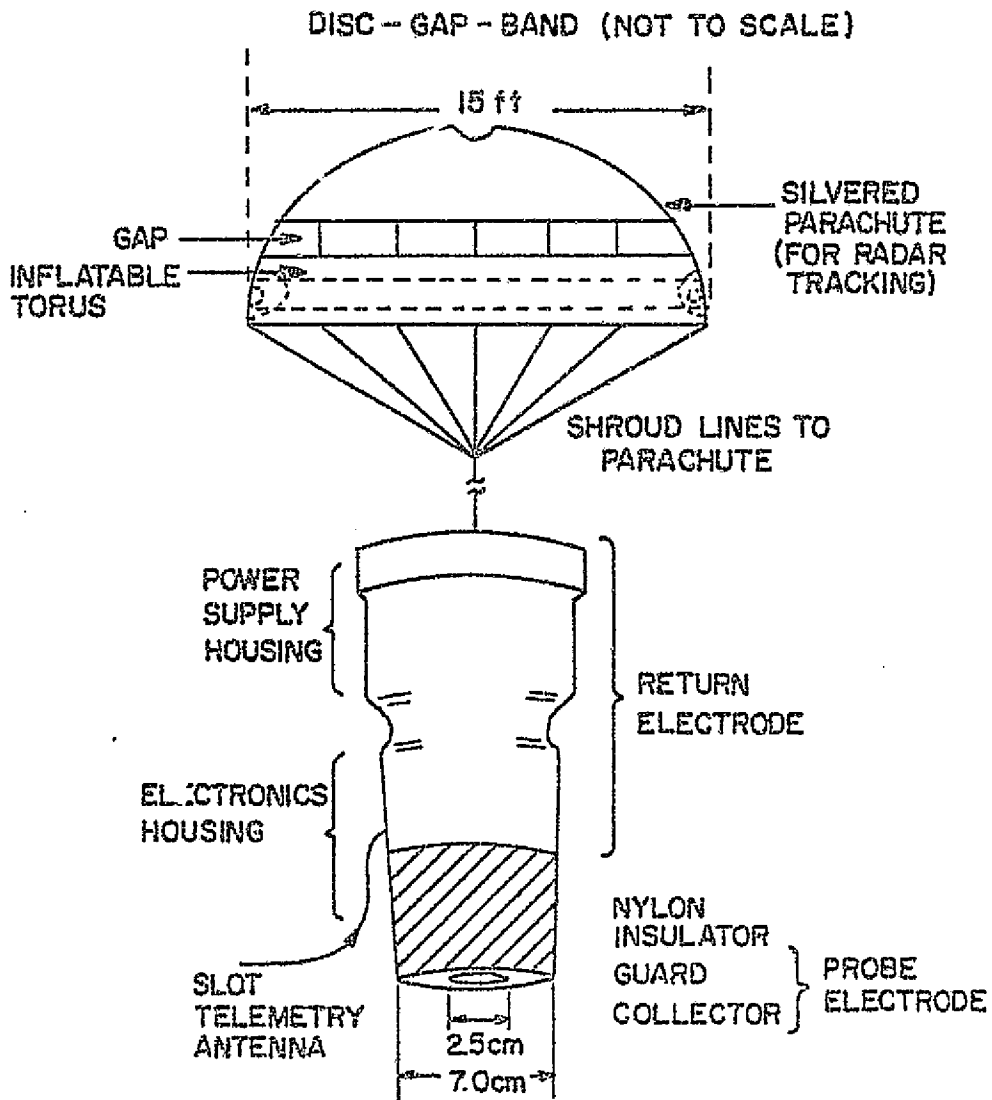


Figure 2.1 The Blunt Probe Assembly

and the current reaching the collecting surface is:

$$I_{p\pm}^+ = 2a^2 V_p \sigma_{\pm}^+ / R \quad (2.5)$$

where σ_{\pm}^+ are the conductivities in the ambient plasma.

Conductivities are determined from $dI_{p\pm}^+ / dV_p$, rather than $I_{p\pm}^+ / V_p$, to remove drift errors in the instrument. V_p is produced by applying a linear sweep voltage (V_s) between the return electrode and the probe. If V_p is greater than a few volts,

$$\frac{dI_{p\pm}^+}{dV_p} \approx \frac{dI_{p\pm}^+}{dV_s} \quad (2.6)$$

and hence, equation (2.5) becomes:

$$\sigma_{\pm}^+ \approx \frac{R}{2a^2} \frac{dI_{p\pm}^+}{dV_s} \quad (2.7)$$

Calibration and conductivity data are converted from telemetry tape to a strip chart recording of current as a function of time. $dI_{p\pm}^+ / dV_s$ is computed from the slope of these curves and is given by:

$$\frac{dI_{p\pm}^+}{dV_s} = \frac{1}{R_{cal}} \frac{(dI_{p\pm}^+ / dt)}{(dI / dt)_{cal}} \quad (2.8)$$

where R_{cal} is the calibration resistance. This equation refers to a ground-based calibration in which the sweep voltage is applied through R_{cal} to the electrometer.

Therefore, equation (2.7) becomes:

$$\sigma_{\pm}^+ = \frac{R}{2a^2 R_{cal}} \frac{(dI_{p\pm}^+ / dt)}{(dI / dt)_{cal}} \quad (2.9)$$

enabling us to obtain σ_{\pm} independent of the sweep amplitude.

Figure 2.2 shows typical voltage and current characteristics of the probe experiment.

Since radar constantly observes the probe's position, the conductivity can be plotted as a function of altitude, Z .

The main advantage of the blunt probe, over slender body geometries such as the Gerdien condenser is that its collection efficiency is much less sensitive to angle of attack on descent and, therefore, less likely to be affected if the probe package is swinging at the end of the parachute after deployment.

The most significant problem with the blunt probe technique is that it measures only conductivity and not number density. A properly selected average mobility is a reasonable way to attack this problem (Mitchell, 1973).

Another problem concerns contamination from the probe itself, i.e. by outgassed water vapor. The result would be to hydrated ions, thereby decreasing their apparent mobility and lowering the measured conductivity (Mitchell, 1973). However, ion conductivity measurements on geophysically similar days are similar, indicating that contamination due to water vapor is not significant (Mitchell, 1973).

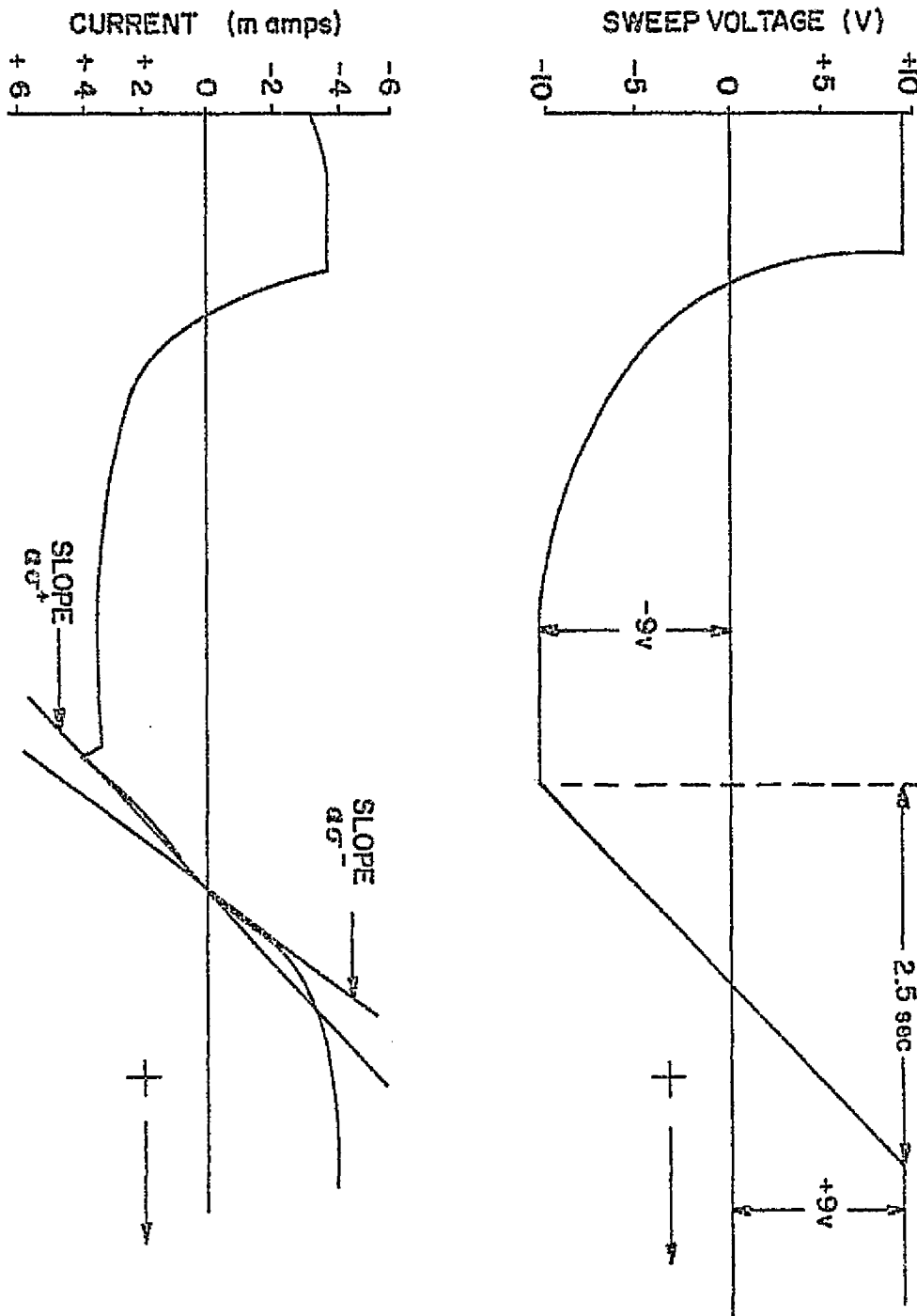


Figure 2.2 Sweep Voltage and Typical Telemetered Current

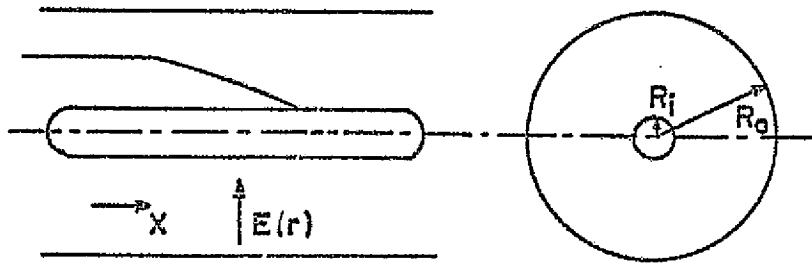
Finally, photo-emission on the collecting surface does not appear to be a significant source of error, since this surface is virtually always shielded from direct sunlight.

2.3 The Gerdien Condenser

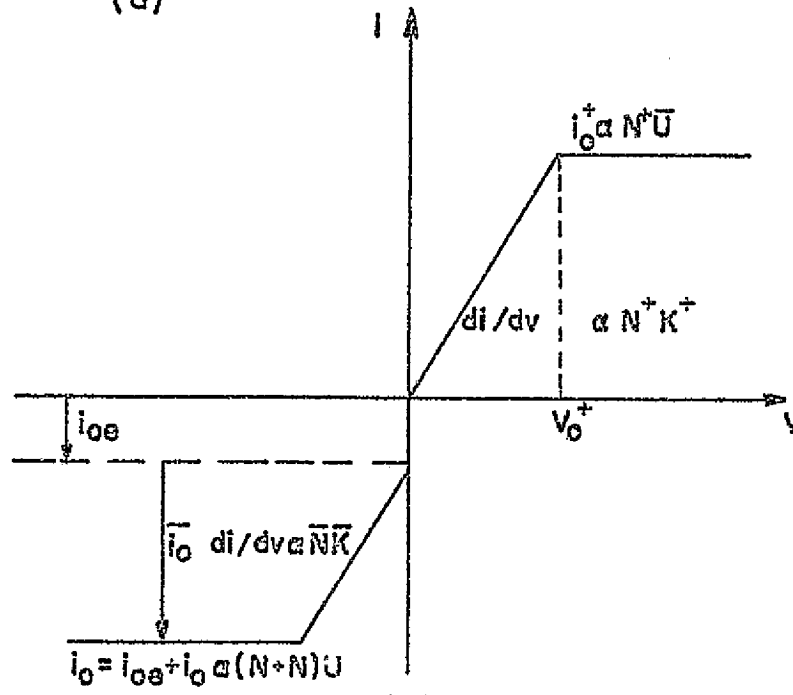
The other simple type of instrument used in measuring the electrical properties of the middle atmosphere is the Gerdien condenser. This device, first constructed by H. Gerdien in 1905, consists of two concentric cylinders positioned so that air flows through the apparatus. At sufficiently low potential difference between the inner and outer cylinder (Figure 2.3a), ions are collected at a rate depending upon the potential difference across the cavity and flow rate through it.

The theoretical current-voltage characteristics of the simple Gerdien condenser geometry as shown in Figure 2.3a are well known. As in the blunt probe technique discussed above, this device also uses a simple mobility mechanism. A sweep voltage is applied between the cylinders and an electrometer measures the resulting collector current. Figure 2.3b shows a typical I-V curve for a gas of single ion mobilities.

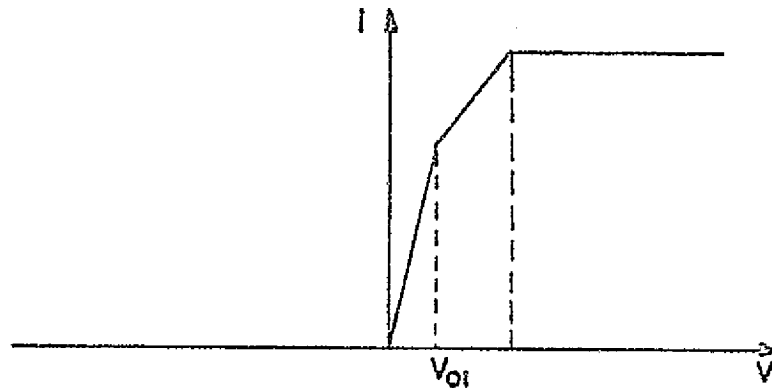
If there are many type ions at different densities and mobilities the I-V characteristics may be obtained by superposition. The current obtained before saturation is (Farrokh, 1975):



(a)



(b)



(c)

Figure 2.5 A Simple Gerdien Condenser

$$I = e \frac{C}{\epsilon} V \sum^n M_n N_n \quad (2.10)$$

where I is the current; ϵ is the permeability of the medium; n is the number of ion species; $C = \frac{2\pi\epsilon L}{\ln(R_0/R_1)}$ is the capacitance of the Gerdien condenser; L is the length of the cylinder; and R_0 and R_1 are radii of the outer and inner cylinders.

Since the number of ions in the flow sample is finite, the instrument has a saturation current, i.e. increased voltage will not produce a similar increase in current and the I-V characteristic becomes nonlinear. For a single type ion species, the negative saturation current I^- is proportional to $\bar{U}(N^- + N)$ where N is electron density and U is the average stream velocity.

After saturation, equation (2.10) has the form:

$$I_0 = e \frac{C}{\epsilon} V_0 \sum^n M_n N_n \quad (2.11)$$

where V_0 is the saturation voltage.

Figure 2.3c shows the I-V characteristics of a Gerdien condenser collecting two types of positive ions. Here, the saturation current, I_0 , is proportional to $\bar{U}(N_1^+ + N_2^+)$. The derivative of the current-voltage characteristic is proportional to $N_2\mu_2$ for $V_{01} < V < V_{02}$.

The ion conductivity, $N^+ e \mu_+$, can be calculated from the slope of the I-V characteristic, since, from equation (2.10), $\frac{dI}{dV} = \sigma \frac{C}{\epsilon}$, and $N^+ \bar{U}$ can be obtained from the saturation current. N^+ or \bar{U} must be known (or assumed) to obtain values of μ_+ .

The Gerdien can be operated as a mobility spectrometer as demonstrated in Figure 2.3c. It is necessary to have an accurate I-V characteristic to distinguish ions of different mobilities.

If ions of one polarity collect more quickly than others of opposite polarity, a space charge will be present between the two electrodes of the condenser, and may distort the electric field in the condenser. Farrokh (1975), however, shows that significant errors due to a space charge effect do not occur below an altitude of 80 Km. Photo-emission on the collector surface does not seem to present serious problems either.

The obvious disadvantage of this device is its high sensitivity to the angle of attack, although better parachute design lessens the severity of this effect.

The main point to consider, however, is that the Gerdien method gives a direct measurement of ion density and conductivity. The blunt probe technique yields the charged particle conductivities, but to deduce ion density, the mobility, μ , must be known. Since the ion mobilities in the lower ionosphere are unknown, the blunt probe technique is not reliable in obtaining density measurements.

2.4 Comparison of Blunt Probe and Gerdien Condenser Measured Conductivities

As part of this research effort, blunt probe and Gerdien measured conductivities obtained during geophysically similar days and times were compared. This was done to examine the reliability of not only the Gerdien positive conductivities, but also of the Gerdien positive ion density. The latter will play an important role in subsequent discussions presented in this report.

Drawn on Figure 2.4 are the positive ion conductivity curves as measured by a blunt probe on 23 May at 1430 EST and a Gerdien on 28 May at 1630 EST. The observed values agree fairly well below 55 Km, but are noticeably different between 55 and 70 Km. Similar comparisons of the Aladdin (1974) campaign data show much better correspondence between the blunt probe and Gerdien data (Leiden, 1976). The differences observed in the Peru data are still unexplained at this time.

Fortunately, the measurement of ion number density with the Gerdien is more reliable than conductivity measurements. This is true since, as discussed in Section 2.2-2.3, the N^+ values are derived from the saturation currents, while the positive conductivities are derived from the slope of the current-voltage characteristics which suffer from drift of zero errors. So, even though a difference in measured conductivities exist, the Gerdien number densities are probably more in line with the blunt

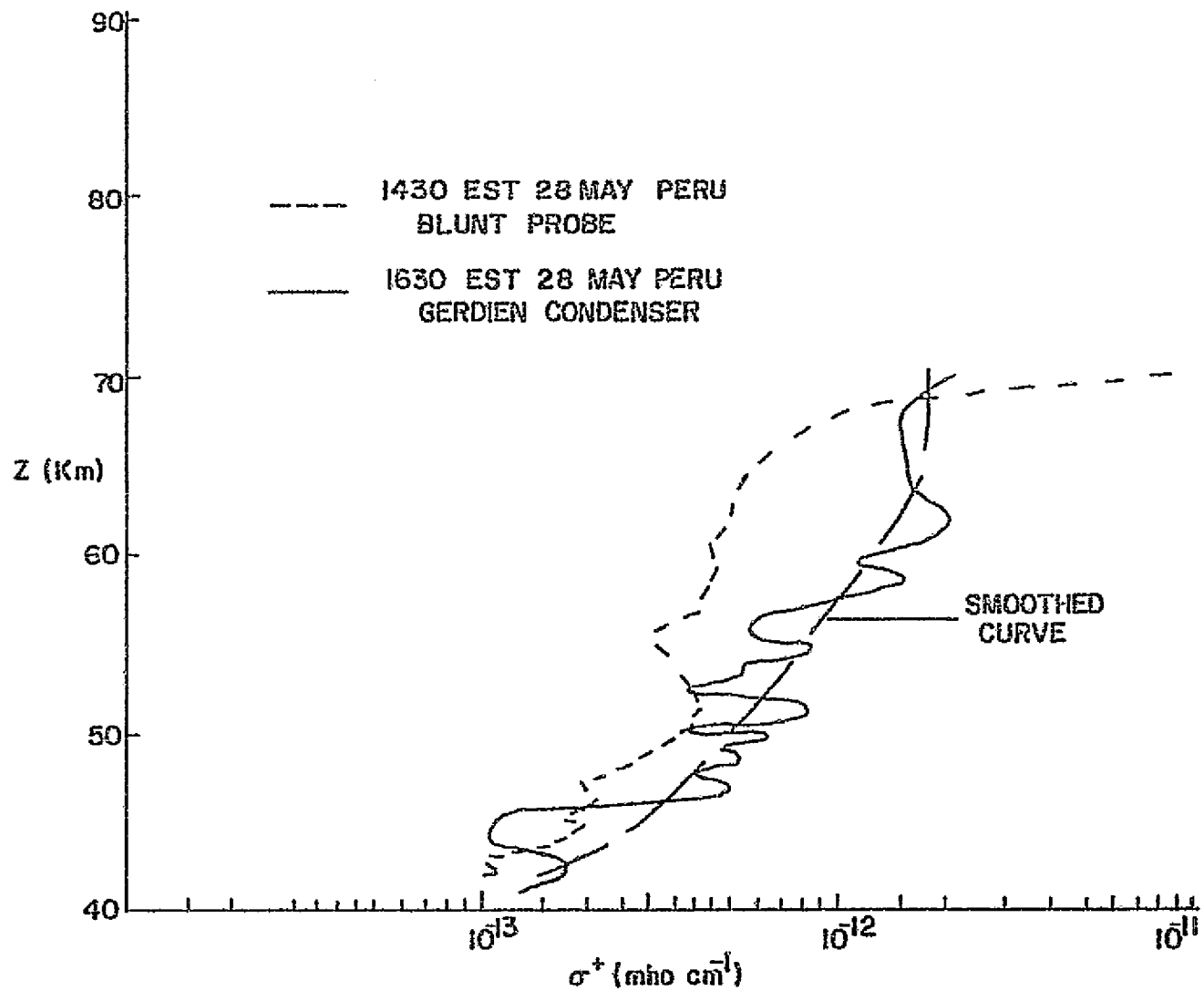


Figure 2.4 Comparison of Blunt Probe and Gerdien Condenser Measured Positive Conductivities

probe conductivity measurements and, therefore, it will be these positive ion densities that will be used in a theoretical analysis of the problem in a subsequent section.

CHAPTER III
EXPERIMENTAL RESULTS

3.1 Conductivity Profiles

As part of the "Antarqui" D-region study, held in May, 1975 in Peru, three blunt probe and one Gerdien condenser instruments designed and constructed here at The Ionosphere Research Laboratory under the guidance of Dr. L. C. Hale were flown in an effort to obtain conductivity and density measurements of the low latitude middle atmosphere. A large number of other measurements were performed by other groups and regular meteorological observations were made as part of this study, making it possible to obtain a "snapshot" of the upper atmosphere during this period. This is especially important since these measured quantities are usually dependent upon a number of diverse parameters.

The instruments were launched at different times, at the Chilca Rocket Range, using Super-Arcas sounding rockets as launch vehicles. The latitude and longitude of the experiment at the Chilca Rocket Range was $12^{\circ}13'15''S$ and $76^{\circ}47'20''W$, respectively. The observed data is now presented and discussed in some detail.

Figure 3.1 shows the measured conductivities for the three blunt probe measurements of the 28th (1430 EST), 23rd (2007 EST), and 24th (0200 EST) of May respectively. (Appendix I lists the mini-computer program that calculates and plots these conductivities from the raw

data using the procedure outlined in Chapter II.) They correspond to a mid-day, late afternoon, evening and late night environments. Smooth curves have been constructed to best fit measured values. Only on the 1430 EST, 28 May flight was information obtained on negative conductivity. Figure 3.2 shows a comparison of the three blunt probe measurements with an average mid-latitude day (Hale, 1973) and a nighttime White Sands Missile Range positive conductivity profile (Mitchell, 1975).

3.2 Discussion of Data

A number of significant points concerning these observations should be noted. On all the daytime profiles, a "knee" occurs at approximately 63 Km. This compares very well with many past measurements of positive conductivity (Hale, 1974) and probably represents physically the altitude at which Lyman α and cosmic ray ionization crossover; the cosmic rays being responsible for the production of ions in the lower, denser atmosphere and the Lyman α radiation ionizing NO above 63 Km. At night, production of ions due to direct Lyman α ceases and the conductivity curve "rises" upward indicating the loss of this ionization source.

It will also be noted that the conductivity is approximately constant for the day measurements in the 50-65 Km altitude range indicating that positive conductivity is relatively independent of atmospheric density. Cipriano

(1973), using statistical techniques, shows that the positive conductivities correlate extremely well with atmospheric temperatures as measured by meteorological "rocket-sondes." He deduces the temperature coefficient of the conductivity increased from 1.7%/°K at 35 Km to 4.6%/°K at 58 Km. The positive conductivity variations do not correlate well with negative conductivity though (Hale, 1973).

On the 0200 EST, 24 May profile, there appears to be wave-like structure in the data from 40 to 50 Km. These may represent equatorial gravity waves in the middle atmosphere: wind data and wavelength considerations bear this hypothesis out (Clark, 1976). Similar structures have not been observed at mid-latitudes, indicating that these short wavelength disturbances are an observable feature of the equatorial upper atmosphere, as predicted theoretically (Holton, 1975).

The 1430 EST, 28 May positive and negative conductivity curves reveal an absence of electrons below 40 Km where the profiles then diverge very rapidly, indicating the presence of many daytime electrons.

The superposition of these profiles in Figure 3.1 yields some interesting results also. The Peru conductivity curves are very similar up to 50 Km or so, then there is an enhancement of the late night curve. The day and evening curves remain fairly constant up to 65 Km where the difference in conductivities arises due to direct Lyman α being present in the day but absent at night.

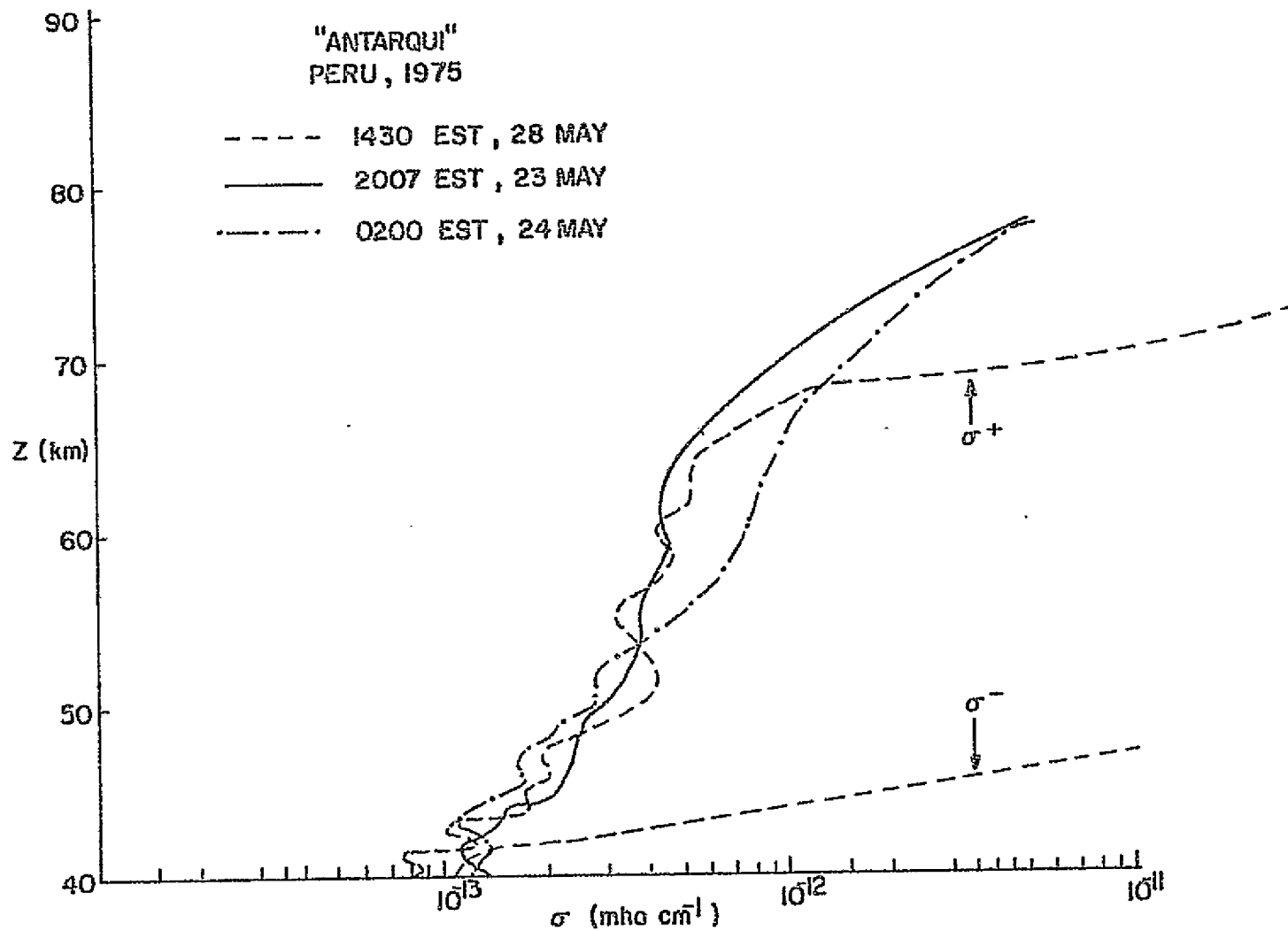


Figure 3.1 Conductivities for 1430 EST, 28 May;
2007 EST, 23 May; and 0200 EST, 24 May, Peru

(We shall see that although scattered Lyman α is present during the night hours, it is insignificant as compared to other sources.) The night and evening curves intersect again, a bit above 75 Km, the region of maximum enhancement being at about 65 Km.

This observation is important since the layer of enhancement, as will be shown in the next chapter, corresponds very well with the altitude range of significant measured, ion production due to celestial X-rays. Here is evidence possibly substantiating the reported effect of celestial X-ray sources upon VLF radio wave propagation (Sharma, et al, 1972). If this enhancement was, on the other hand, related to a return to nighttime steady state conditions, the layer affected is expected to be much deeper, perhaps down to 40 Km. This is certainly not what is observed in Figure 3.1.

Finally, two "typical" mid-latitude conductivity profiles (one day and one evening) were drawn for comparison purposes, Figure 3.2. The "knee" still occurs at 65 Km but the measured conductivities are greater by a factor of 2; this is due to increased cosmic ray production of ionization at more northerly latitudes, as predicted by theory. The observed nighttime enhancement is still about 1.5 times the day conductivities. Interestingly, the altitudes where the nighttime enhancement begins and ends is lower than those observed in the equatorial flights.

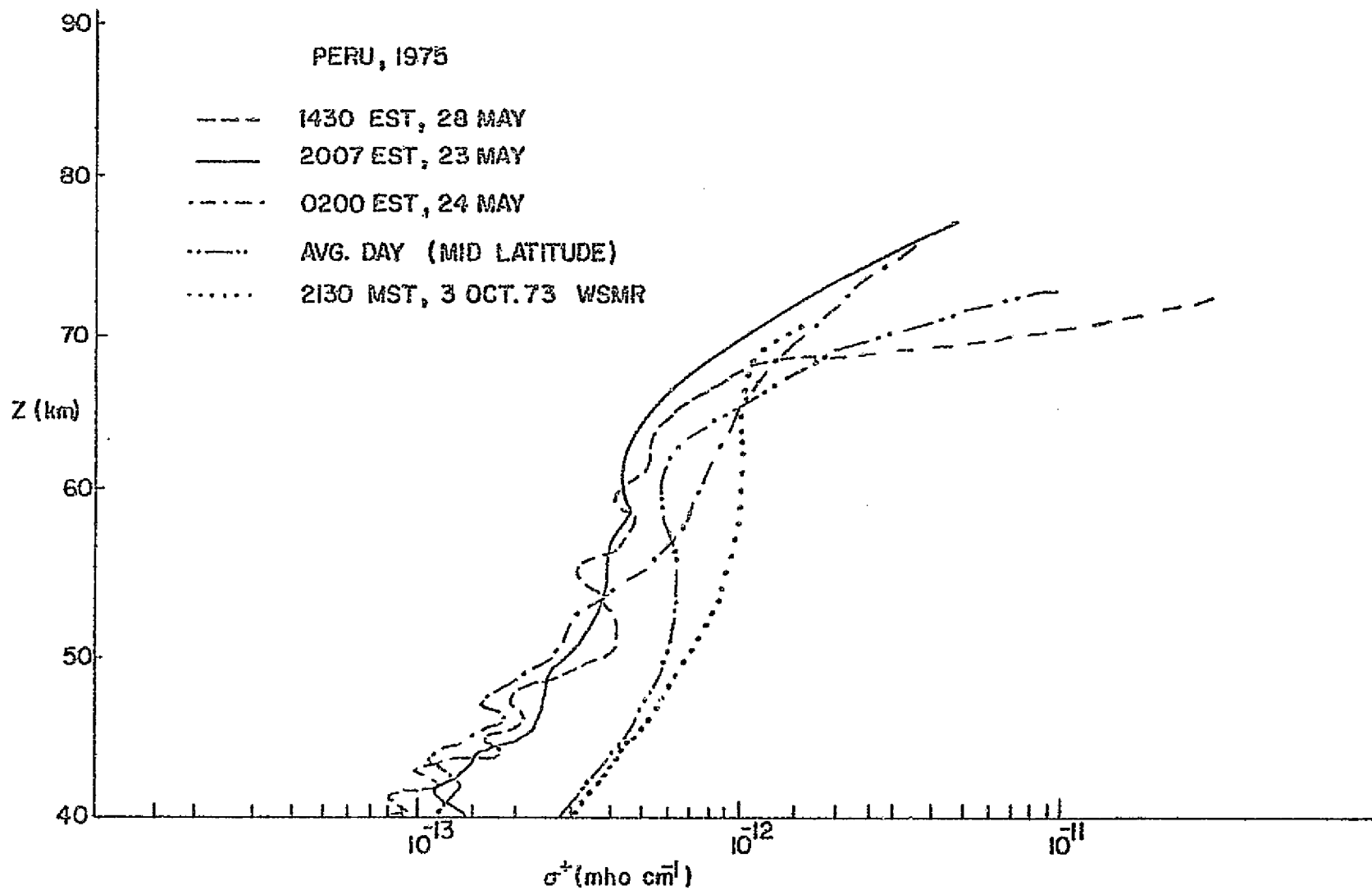


Figure 3.2 Composite of σ^+ Profiles for "Antarqui" (Equatorial) and Mid-latitudes

3.3 Positive Ion Densities

Positive ion concentration was measured directly by a Gerdien condenser on 24 May, 1630 EST, as part of the overall campaign. This data is presented in Figure 3.3 (Leiden, 1976).

Since a comparison of the directly measured Gerdien ion densities and, the derived blunt probe densities is desired, an analysis of the derived positive ion concentration from the blunt probe conductivity follows. If one assumes a small ion model, positive ion densities can be calculated from the measured conductivities by (Hale, 1973):

$$N^+ = \frac{\sigma_+}{e\mu^+} \quad (3.1)$$

where e is the electronic charge and μ the averaged positive ion mobility. Now, the mobility of a single ionic species is (Dalgarno, 1962):

$$\mu = \frac{\mu_0 T_0^P P_0}{T_0^P} \quad (3.2)$$

where P_0 and T_0 are the sea level reference pressure and temperature respectively, and μ_0 is the reduced mobility, i.e. the mobility of the ion species at STP. μ_0 is assumed to be $1.8 \times 10^{-4} \text{ m}^2 \text{ v}^{-1} \text{ s}^{-1}$ for positive ions (Loeb, 1955). Putting equation (3.1) into (3.2):

$$N^+ = \frac{\sigma_+ T_0^P P_0}{e\mu_0 T_0^P} \quad (3.3)$$

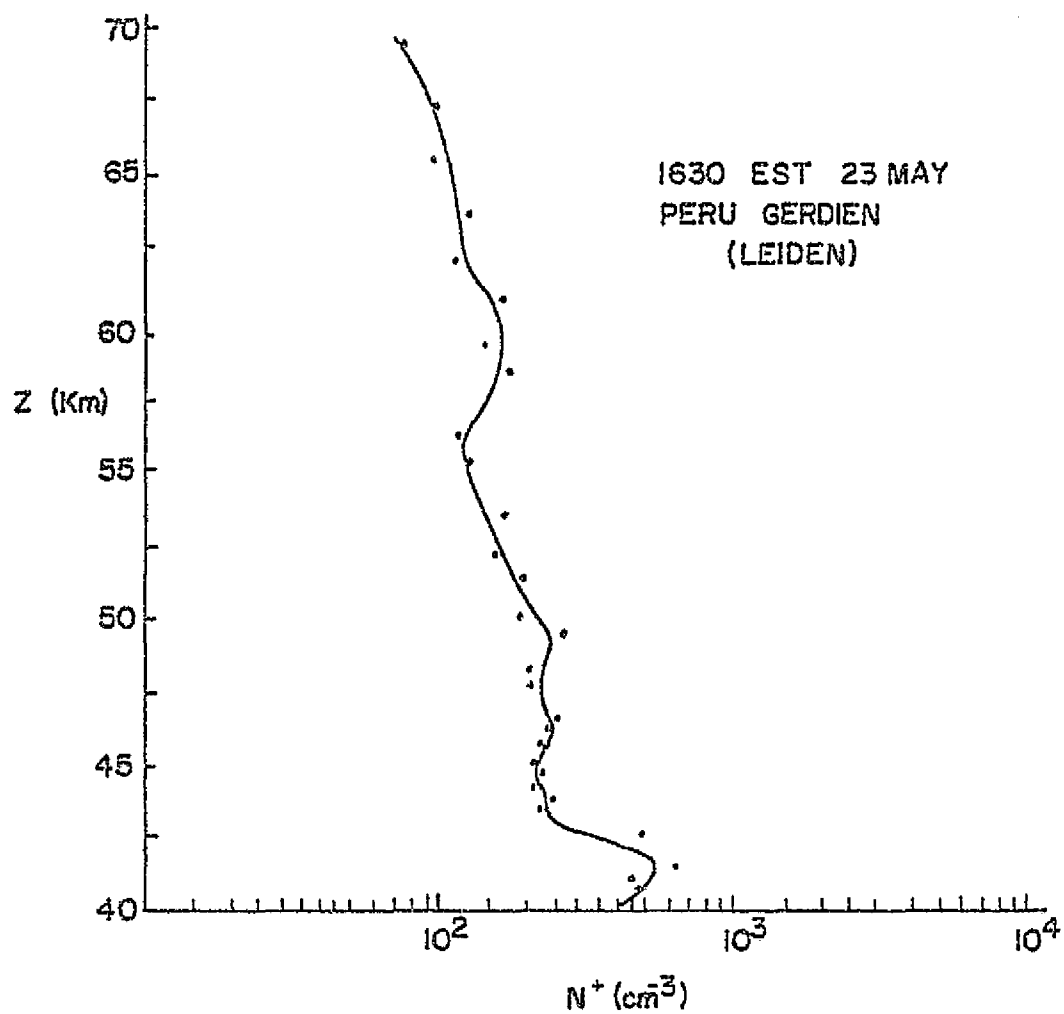


Figure 3.3 Gerdien Ion Densities for
1630 EST, 23 May, Peru

T and P are obtained from meteorological data or, in this case since the rocket-sonde data was questionable, a standard atmosphere. The COSPAR International Reference Atmosphere as listed in the DNA Reaction Rate Handbook (1972) is used, making it possible to obtain positive ion density from only positive conductivity data.

The N^+ 's were calculated as explained above for the 1430 EST blunt probe conductivity data; they are plotted on Figure 3.4. A number of features are to be noticed. The "knee" of the conductivity curve is reflected in the ion density curve as a deep minimum. Again, this is interpreted to be the "crossover" region between Lyman and cosmic ray production. In the 65-50 Km layer, the slope is approximately proportional to air density (CIRA, 1972) indicating large numbers of electrons with a density roughly constant in this range, satisfying the steady state lumped ion continuity equation:

$$Q = \alpha_d N^+ N_e + \alpha_i N^+ N^-$$

where Q is ion production rate and α_d and α_i are the dissociative and ion-ion recombination coefficients (Hale, 1973).

If one compares Figures 3.4 and 3.3, it is obvious that the Gerdien densities and blunt probe calculated densities differ by about a half order of magnitude. It appears that the assumed reduced mobility, u_0 , is incorrect since a small ion model does not seem to agree

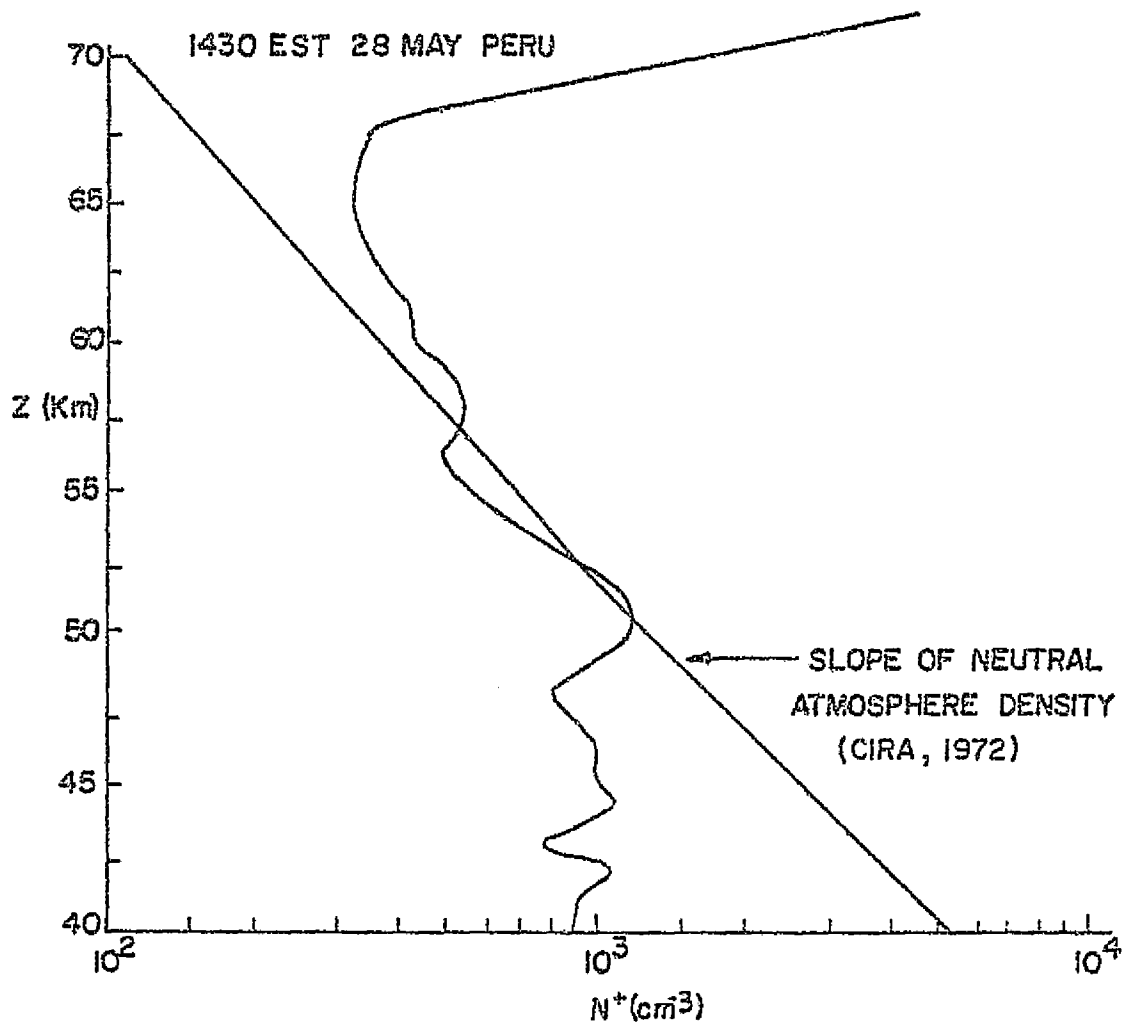


Figure 3.4 Calculated Ion Densities for
1430 EST, 23 May, Peru

with recent experimental results (Hale, 1976), and that obviously large ion models will now have to be considered. It is concluded then that the Gerdien N^+ 's are probably better estimates than those calculated by assumed mobilities, and, thusly, will be used in subsequent calculations requiring ion densities.

3.4 Experimental Errors

In experiments of this type, discussing absolute errors in conductivity measurements is very difficult to say the least. The theory of positive ion collection is well understood and, therefore, a high level of confidence can be put upon positive conductivity data and subsequently derived parameters. Since the collection of negative ions and electrons on the blunt probe surface is a non-linear function of electric field/atmospheric pressure, negative conductivities are difficult to interpret in an absolute sense.

Some general statements can be made about relative errors. Altitude accuracy is usually ± 1 Km or better for all data. Blunt probe data itself is accurate to $\pm 10\%$ for subsonic velocities. Current-slope measurements are $\pm 5\%$ accurate. Geometrical effects and errors in probe potential account for $\pm 10\%$ error. Therefore the absolute accuracy of the conductivity measurements is $\pm 25\%$ (Hale, 1967). The reliability of conductivity ratios is much greater, probably within 10%. Lastly, these errors

are very similar to those in the Gerdien experiment and the estimated accuracy is comparable. This indicates that the data reported does have real physical significance.

The most important fact to note, however, is that all of the curves drawn or mentioned in this chapter have been obtained and reduced in consistent fashion, putting a much higher level of confidence on the values when used for comparative purposes, as we shall indeed do.

CHAPTER IV
THEORETICAL CONSIDERATIONS

4.1 Ionization Sources

The significant sources of lower D-region ionization were briefly mentioned in Section 1.1. In this section, the actual nighttime production rates will be discussed and their relative importance assessed.

Figure 4.1 (adapted from Rowe, 1972) presents the ion-pair production rate of these various sources of nighttime middle atmosphere ionization. The curves represent the production rates as a function of altitude. For the purposes of this research, all the sources will be assumed to be isotropic, although the galactic X-rays may be sensitive to the zenith angles of intense point sources and, possibly, the upper atmosphere itself may act as an X-ray telescope, making the X-radiation non-isotropic.

At 65 Km, the cosmic ray production, which is moderated by the solar activity cycle but fairly constant over shorter time periods, and the balloon measured galactic X-ray production (Barcus, 1975) are equal and represent the most important known ionization sources at this level. Scattered Lyman α , another possible ionization source, would contribute less than 10% of the production, as compared to the above mentioned sources, at 65 Km and drops off very steeply at lower heights.

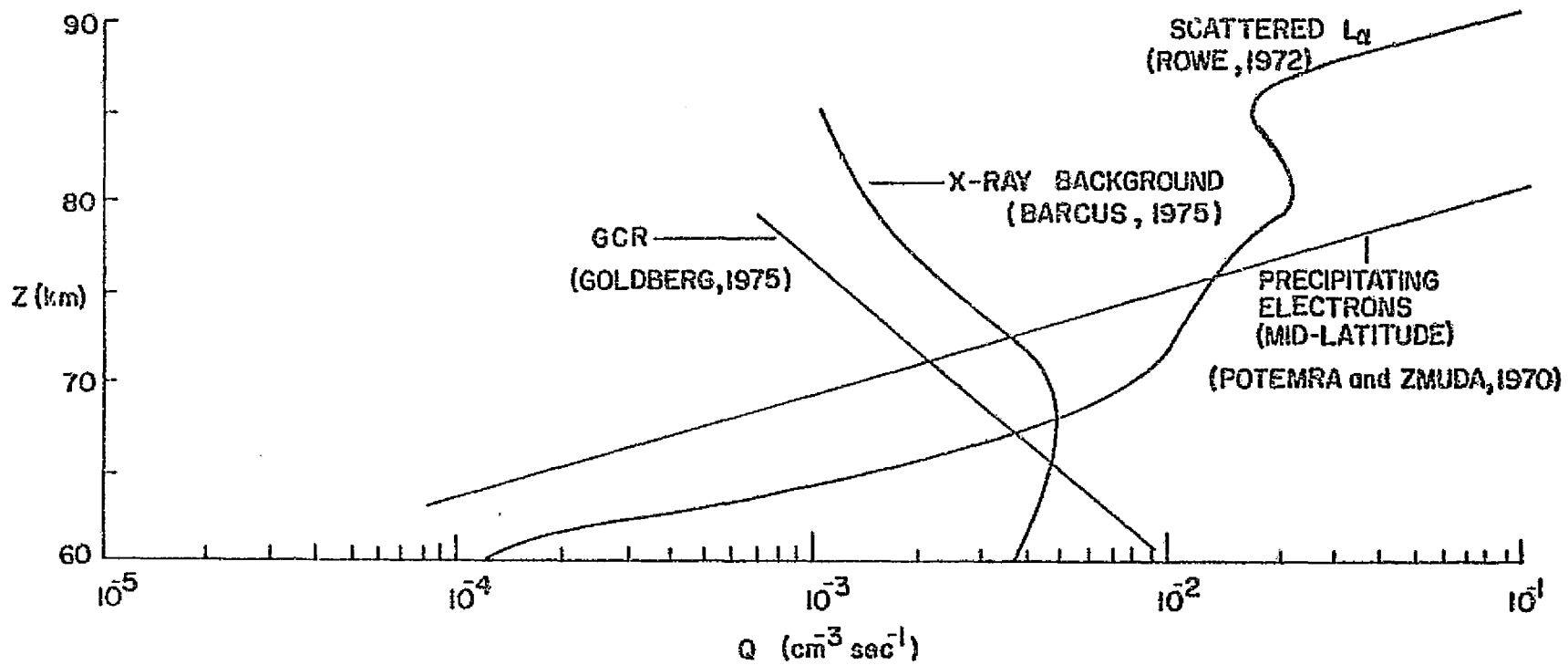


Figure 4.1 Production Rates Due to Various Nighttime Ionization Sources

The X-ray curve decreases rapidly and ceases to be a factor below 40 Km or so. The cosmic ray production increases, proportional to air density, to much lower altitudes (Goldberg, 1975; Velinov, 1968). Finally, the mid-latitude precipitating electron production rate indicates that this is certainly not a significant source below 70 Km (Potemra and Zmuda, 1970).

From these considerations, it appears that the galactic X-ray source should have a definite influence upon middle atmosphere ionization, especially in the 70-50 Km altitude range. However, the matter of an enhancement in ion production due to X-rays is still controversial since most studies have investigated the effects on VLF phase by X-ray sources and this phenomena occurs at a much higher altitude, about 80 Km where ionization is due to a number of sources and it is therefore more difficult to distinguish among them. With this in mind, an attempt has been made to model, in a simple and straightforward manner, the ionization processes in the lower D-region, where it is felt the X-ray source would have a greater effect on production than at 80 Km. The theoretical behavior of the model can be studied, and then compared to the measured conductivity and positive ion number density "diurnal change" in the region of interest, using the ion densities of Figure 3.4 as an initial condition.

4.2 The Continuity Equation

In the lower ionosphere, transport of positive ions can be neglected since the lifetimes of the ions are small as compared to transport times of neutral wind velocities (Rishbeth and Garriot, 1969). Therefore the lumped, effective positive ion continuity equation may be written:

$$\frac{dN^+}{dt} = Q - \alpha_d N^+ N_e - \alpha_i N^+ N^- \quad (4.1)$$

where N^+ is the positive ion density; Q is the total ion production rate; α_d is the dissociative recombination coefficient; and α_i is the ion-ion recombination coefficient.

Under nighttime conditions there are no electrons present and equation (4.1) becomes:

$$\frac{dN^+}{dt} = Q - \alpha_i N^+ N^- \quad (4.2)$$

Finally, assuming $N^+ = N^-$ we have:

$$\frac{dN^+}{dt} = Q - \alpha_i N^2 \quad (4.3)$$

This equation will now be solved and then used to calculate the time dependence of the positive ion concentration.

4.3 Solution of the Continuity Equation

Equation (4.3) has the general solution

$$N^+(t) = \left(\frac{Q}{\alpha_i}\right)^{1/2} \tanh\left[\tanh^{-1}\left(n_0 \frac{\alpha_i}{Q}\right) + t(\alpha_i Q)^{1/2}\right] \quad (4.4)$$

where n_0 is the initial value of N^+ (positive ion density) and here serves as a boundary condition of this differential equation (Nawrocki and Papa, 1961).

Equation (4.4) can be solved numerically by logarithmic expansions of the form:

$$\tanh^{-1} x = \frac{1}{2} \ln \left(\frac{1+x}{1-x} \right) \quad (4.5)$$

if $-1 < x < 1$, and

$$\tanh x = \frac{e^x - e^{-x}}{e^x + e^{-x}} \quad (4.6)$$

4.4 Analysis of Calculated Ion Density Versus Time Profiles

The N^+ versus time profiles for each of the altitudes 55 - 65 Km were calculated using the equations of Section 4.3 and the Gerdien measured densities at 1630 EST, 28 May as n_0 , the initial ion density. Two values of Q , $Q_{\text{cosmic ray}}$ and $Q_{\text{cosmic ray+X-ray}}$, and varying reasonable values of α_i were employed in this procedure. Four parameters in these calculations are presumed to be well known, $Q_{\text{cos ray}}$, $Q_{\text{X-ray}}$, and the initial and final positive ion concentrations. Here, it is assumed that the measured X-ray production rates, and this measurement was made only once, pictured in Figure 4.1 are constant. Since the 1430 EST and 2007 EST conductivities had little variation below 65 Km, it was assumed that the 1630 EST Gerdien densities would be reliable initial conditions. The final N^+ 's, however,

were obtained from the reasonable assumption that $N^+ \propto \sigma^+$ (Hale, 1973) and therefore the increase of N^+ was calculable from the observed enhancement of positive conductivity between 1430 EST and 0200 EST. It is also assumed that by 0200 EST a steady state, or near steady state, condition prevailed in the height range under consideration. With these conditions and assumptions, α_i is the only free parameter.

Figures 4.2 - 4.12 show the result of these calculations. Each solution asymptotically approaches a steady state ion density, N_{ss}^+ , given by:

$$N_{ss}^+ = \left(\frac{Q}{\alpha_i} \right)^{1/2} \quad (4.7)$$

For each of the two values of Q , as labeled, at a given altitude there appear to be a range of α_i that will make the solution approach the observed enhancement of positive ion density, also labeled, within the limits of experimental error.

Further, there will be two pairs of Q and α that will force the solution to approach asymptotically the final or near final N_{ss}^+ observed and have relaxation times also on the order observed, ~ 8 to 10 hours. These "best fit" values from each of the eleven altitudes considered are plotted on Figure 4.13.

Clearly, there is a large difference in the values of α_i with and without the $Q_{X\text{-ray}}$ added to the $Q_{\text{cos ray}}$. Below 58 Km, α_i increases suddenly in both cases, this seeming to indicate a new chemistry is occur-

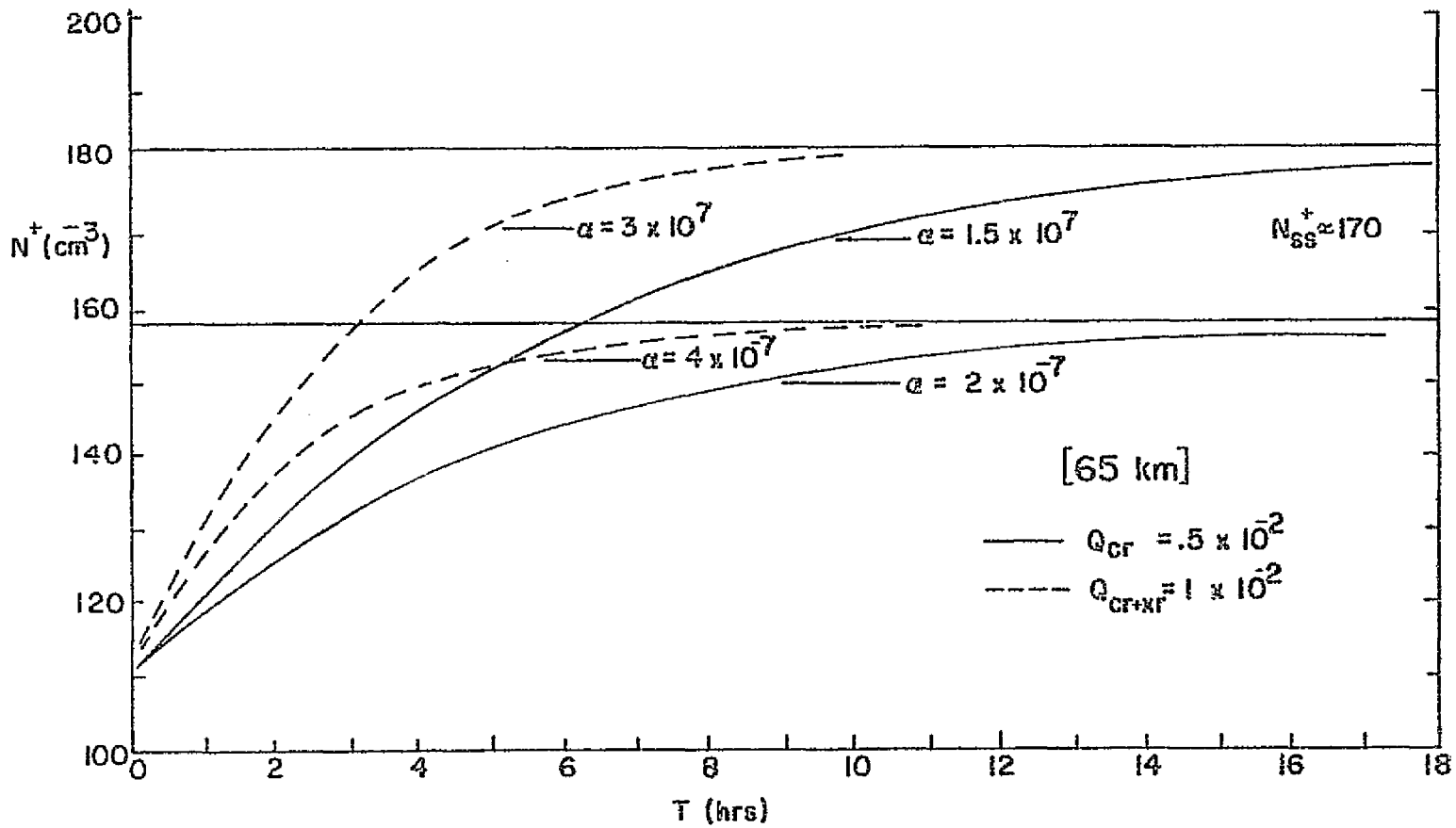


Figure 4.2 N^+ Versus Time at 65 Km

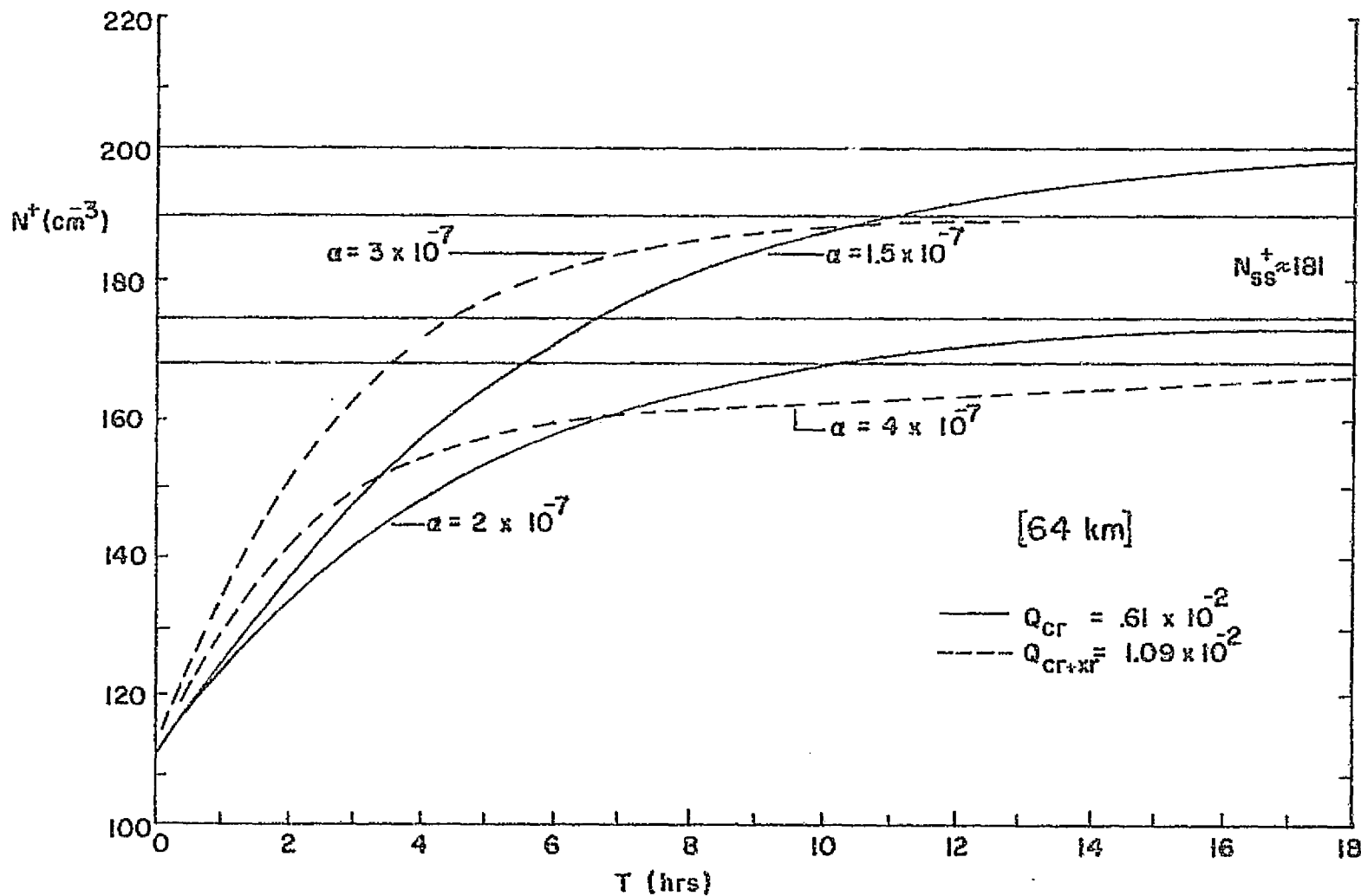


Figure 4.3 N^+ Versus Time at 64 Km

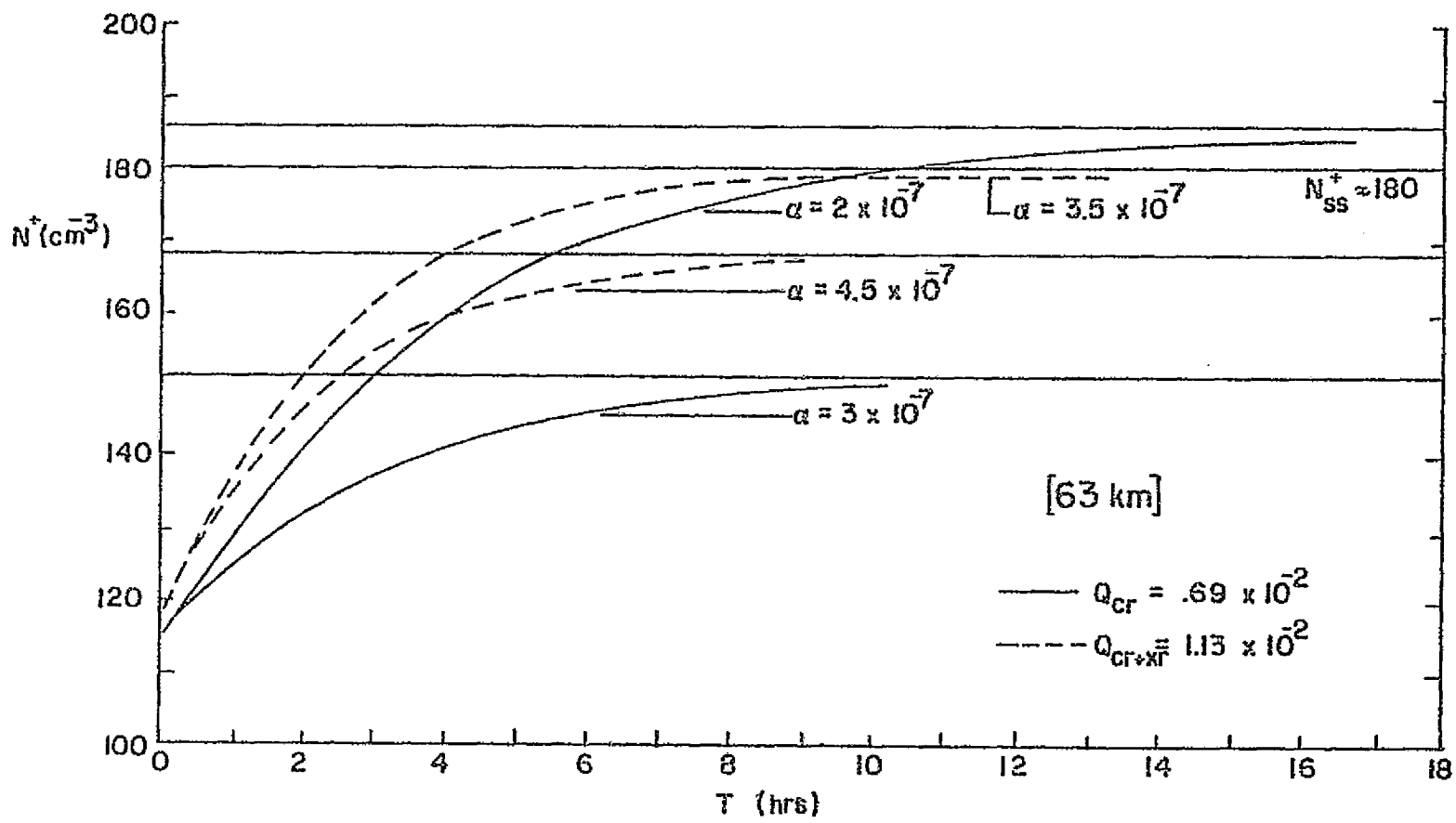


Figure 4.4 N^+ Versus Time at 63 Km

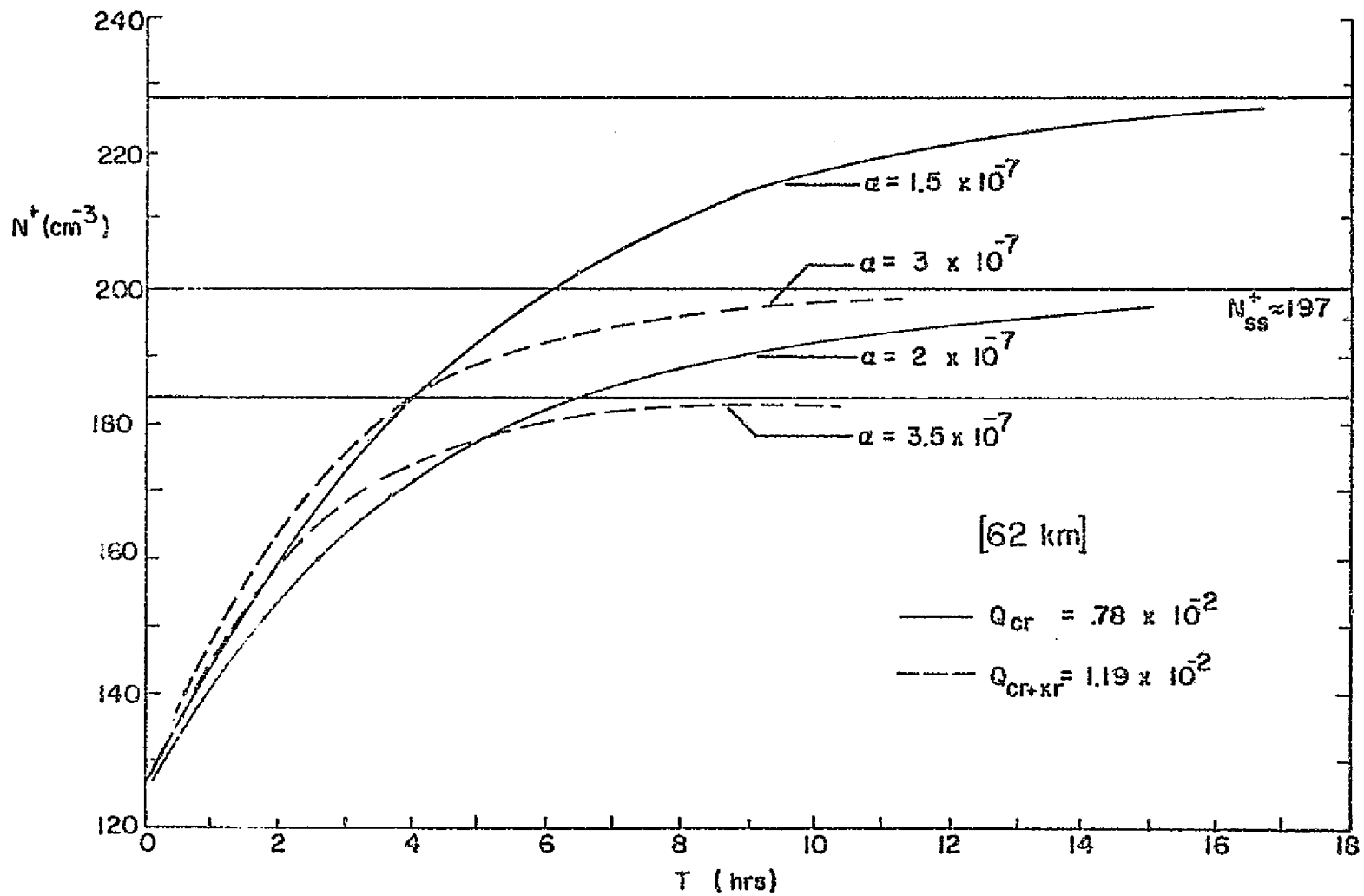


Figure 4.5 N^+ Versus Time at 62 Km

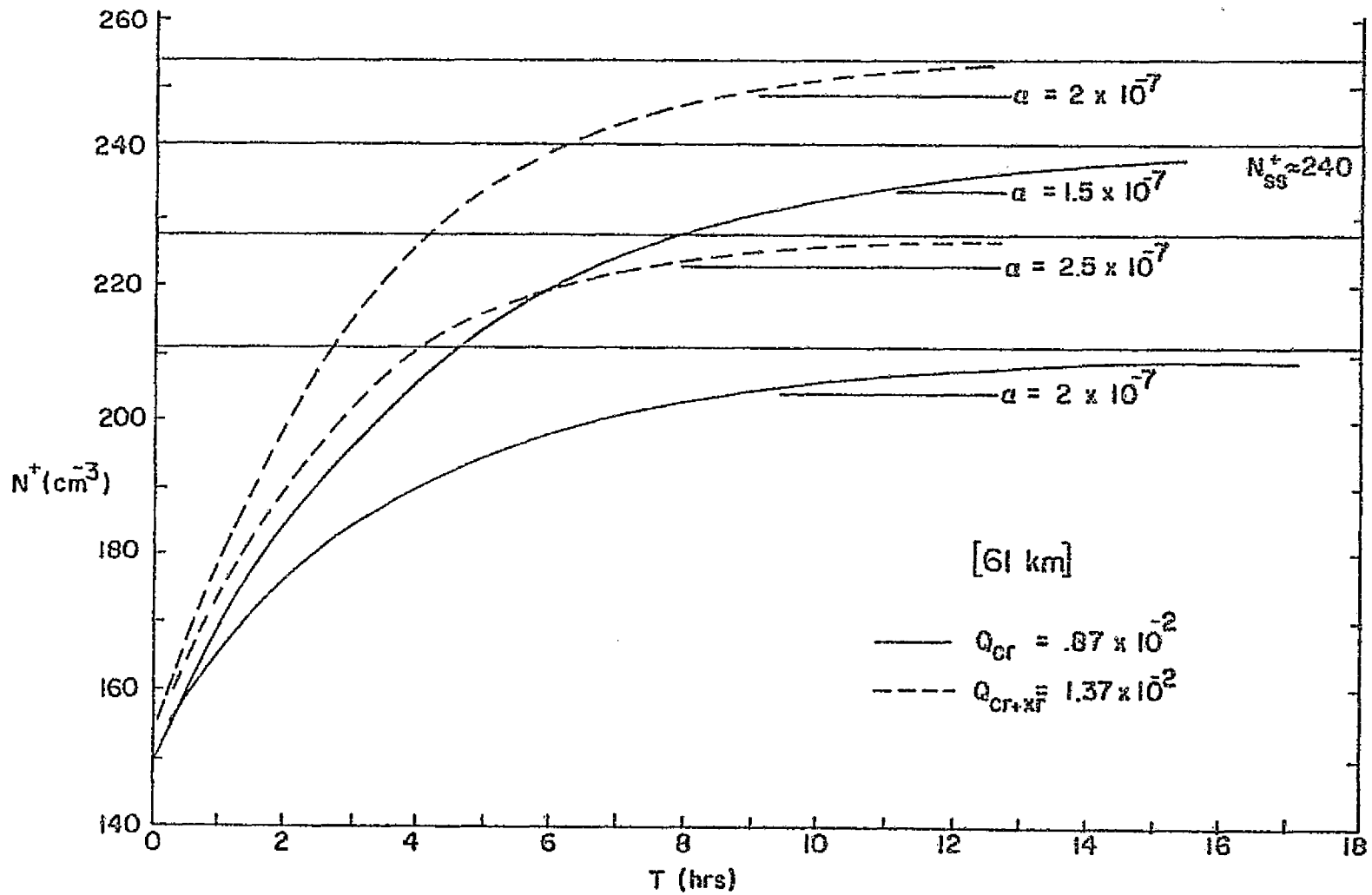


Figure 4.6 N^+ Versus Time at 61 Km

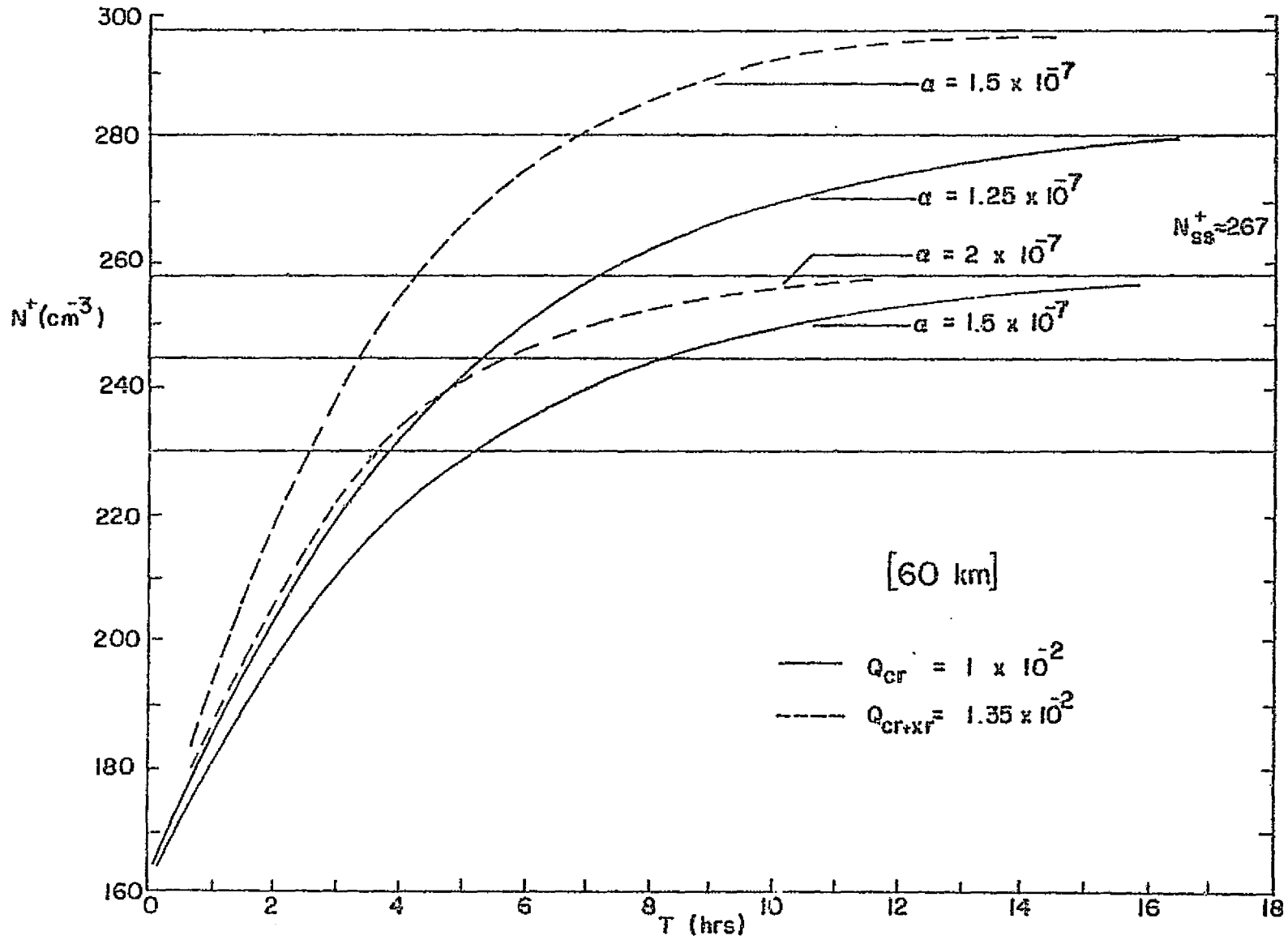


Figure 4.7 N^+ Versus Time at 60 Km

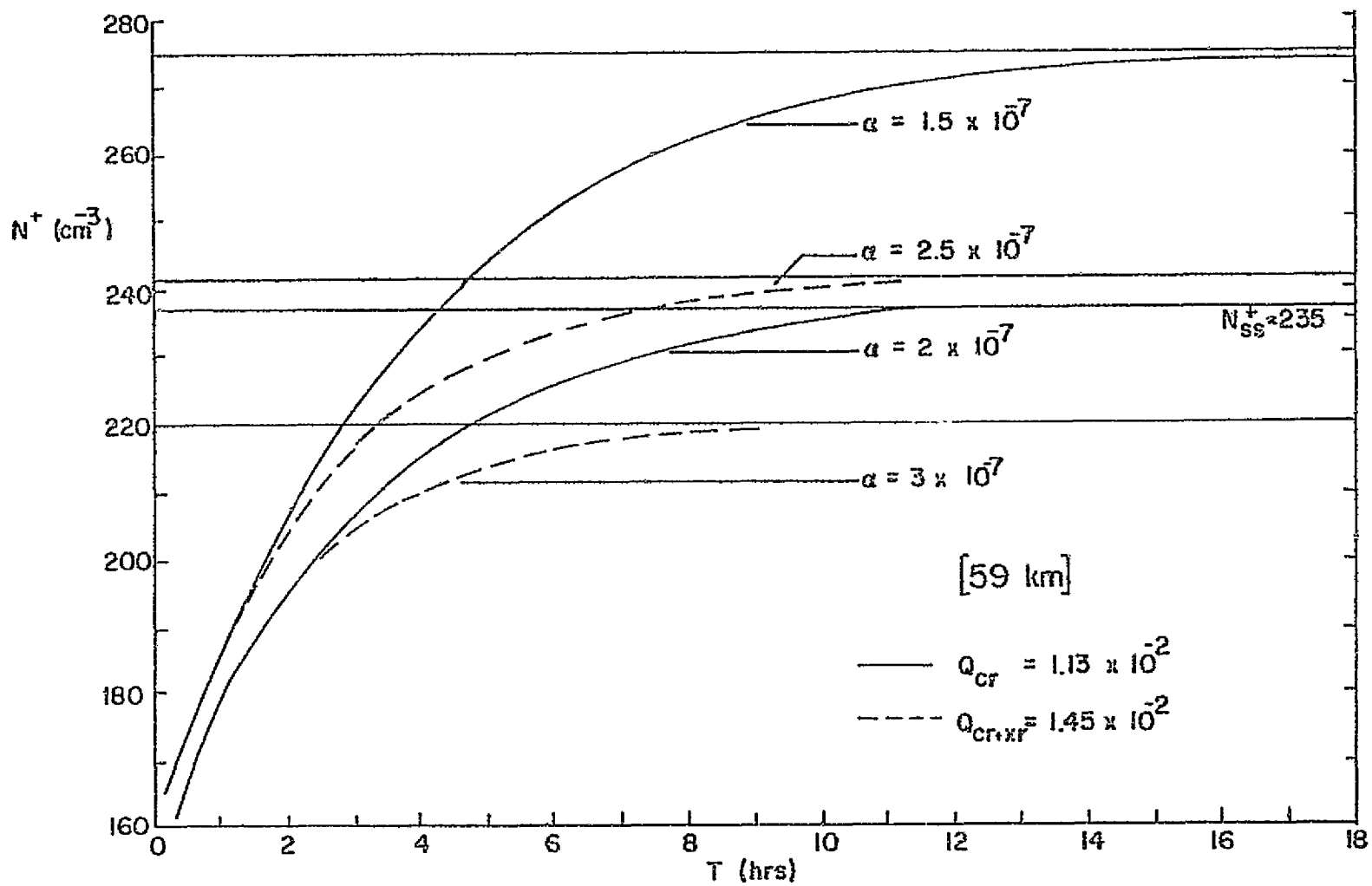


Figure 4.8 N^+ Versus Time at 59 Km

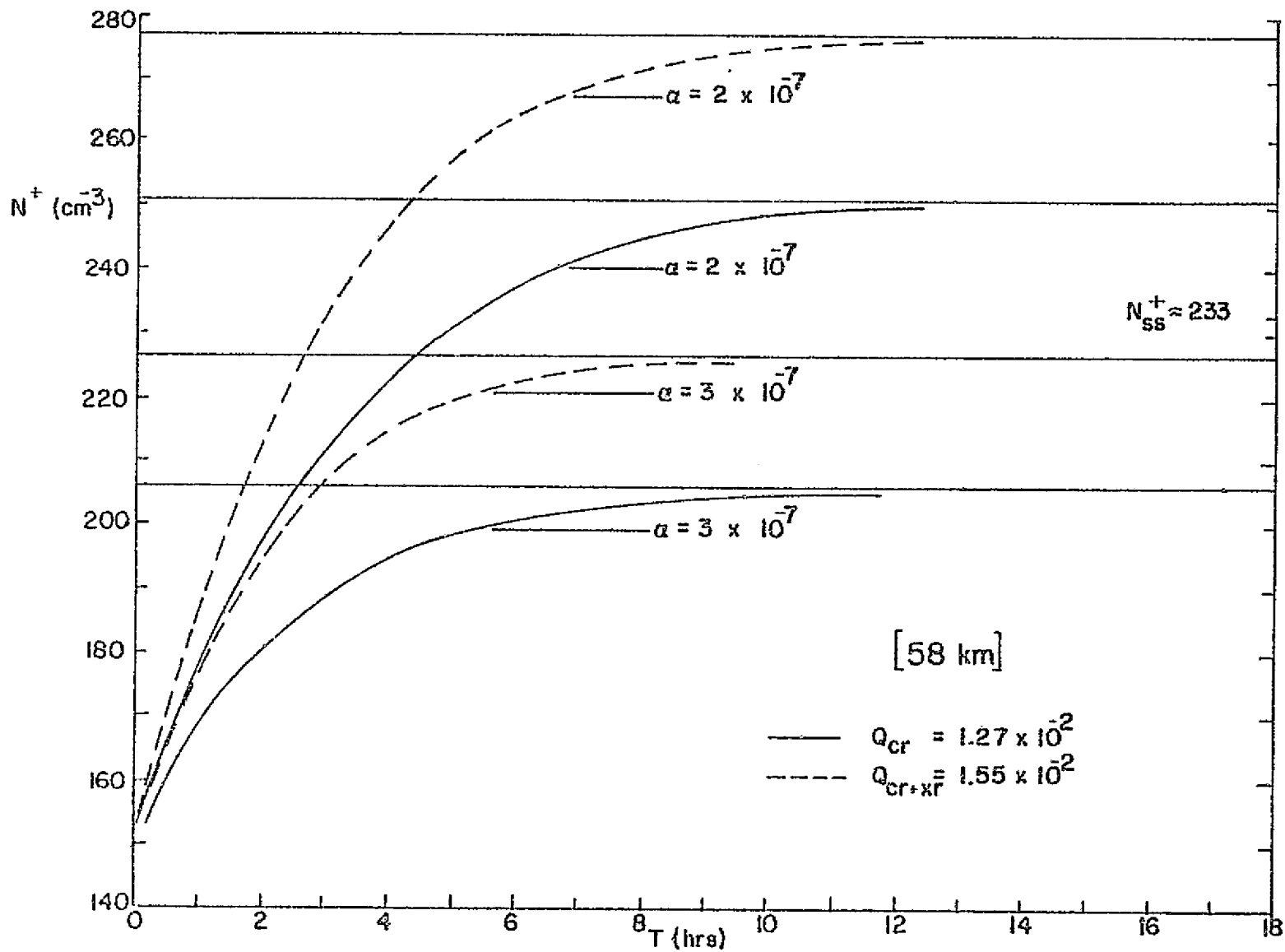


Figure 4.9 N^+ Versus Time at 58 Km

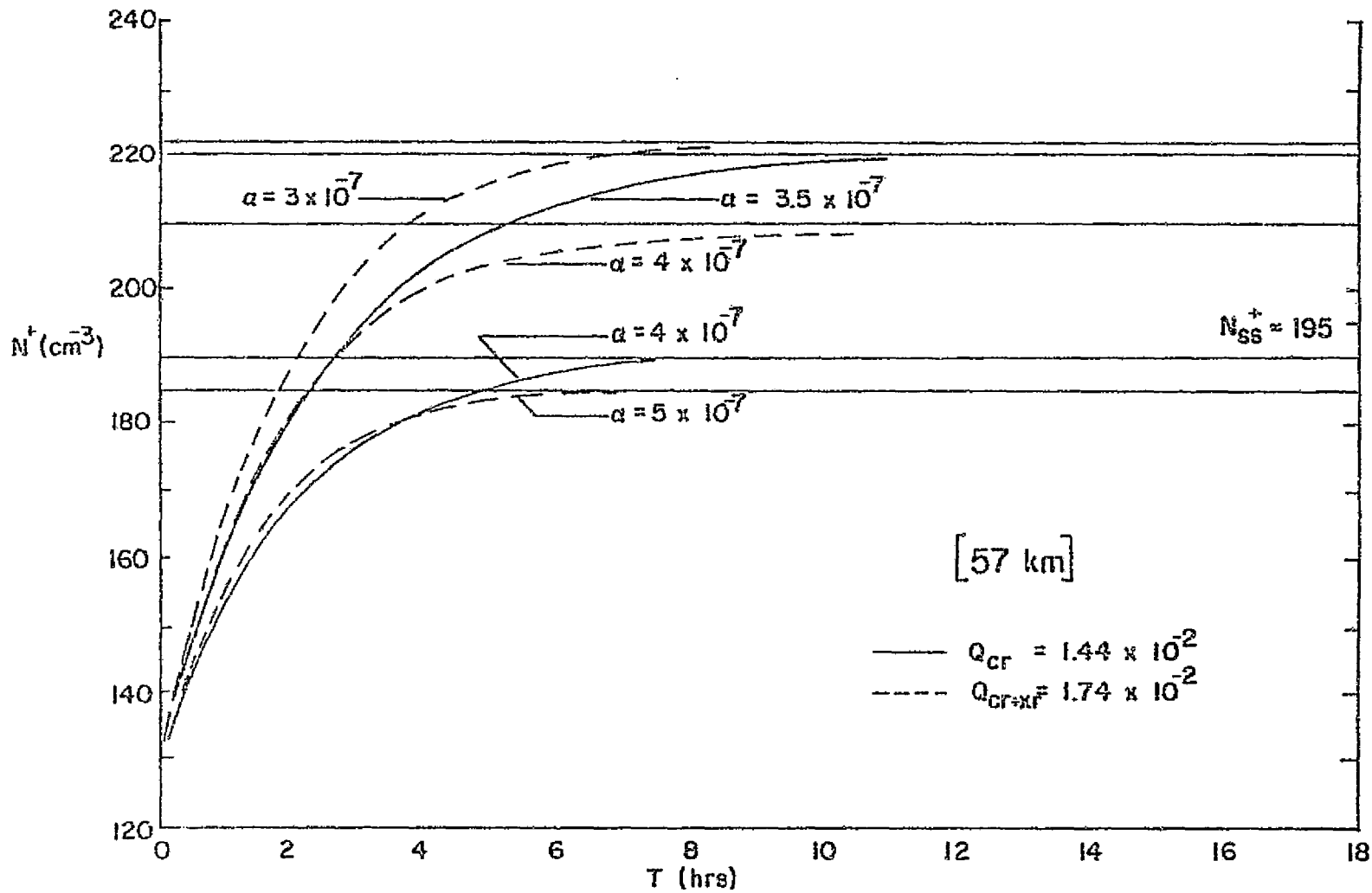


Figure 4.10 N^+ Versus Time at 57 Km

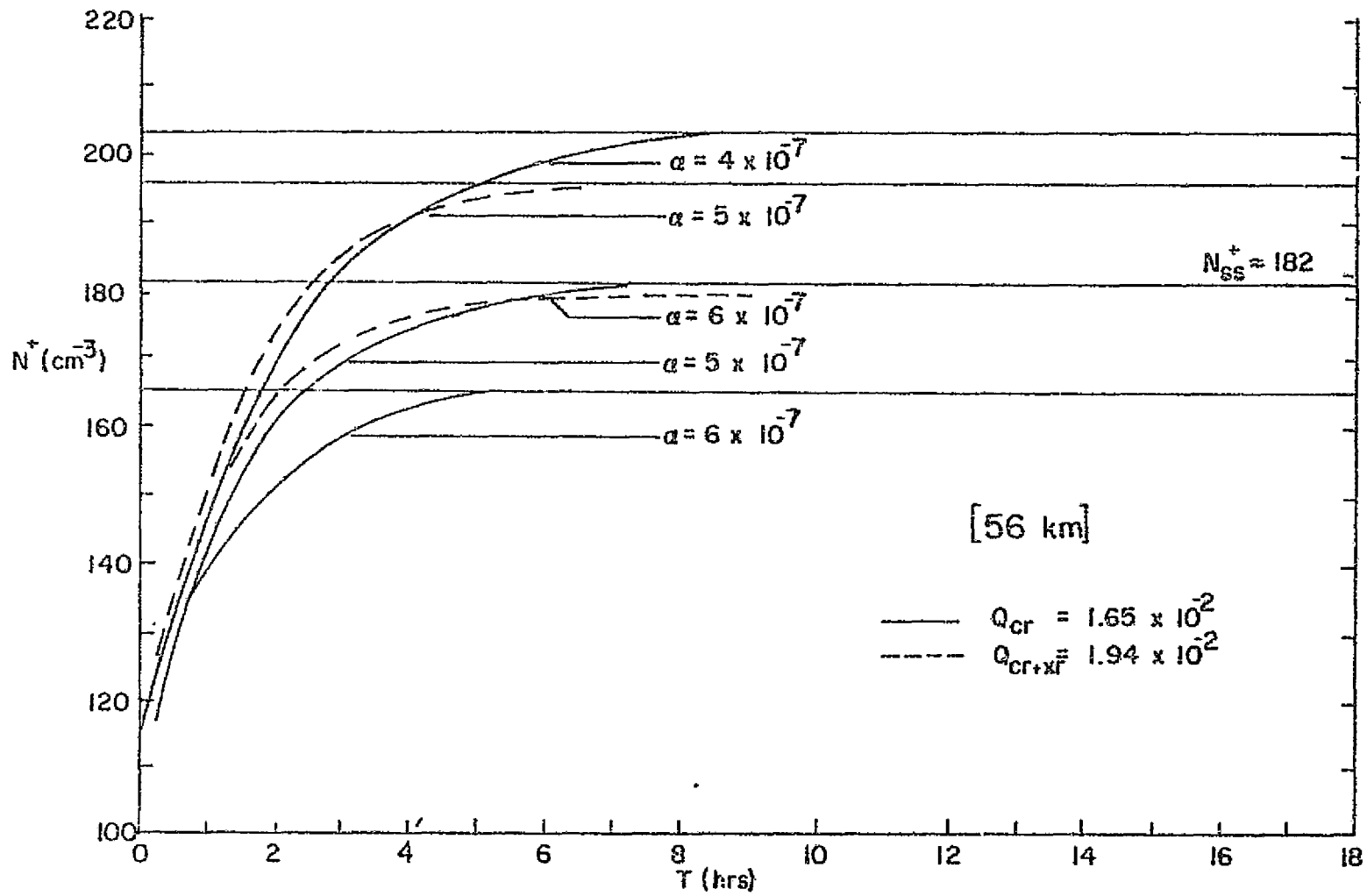


Figure 4.11 N^+ Versus Time at 56 Km

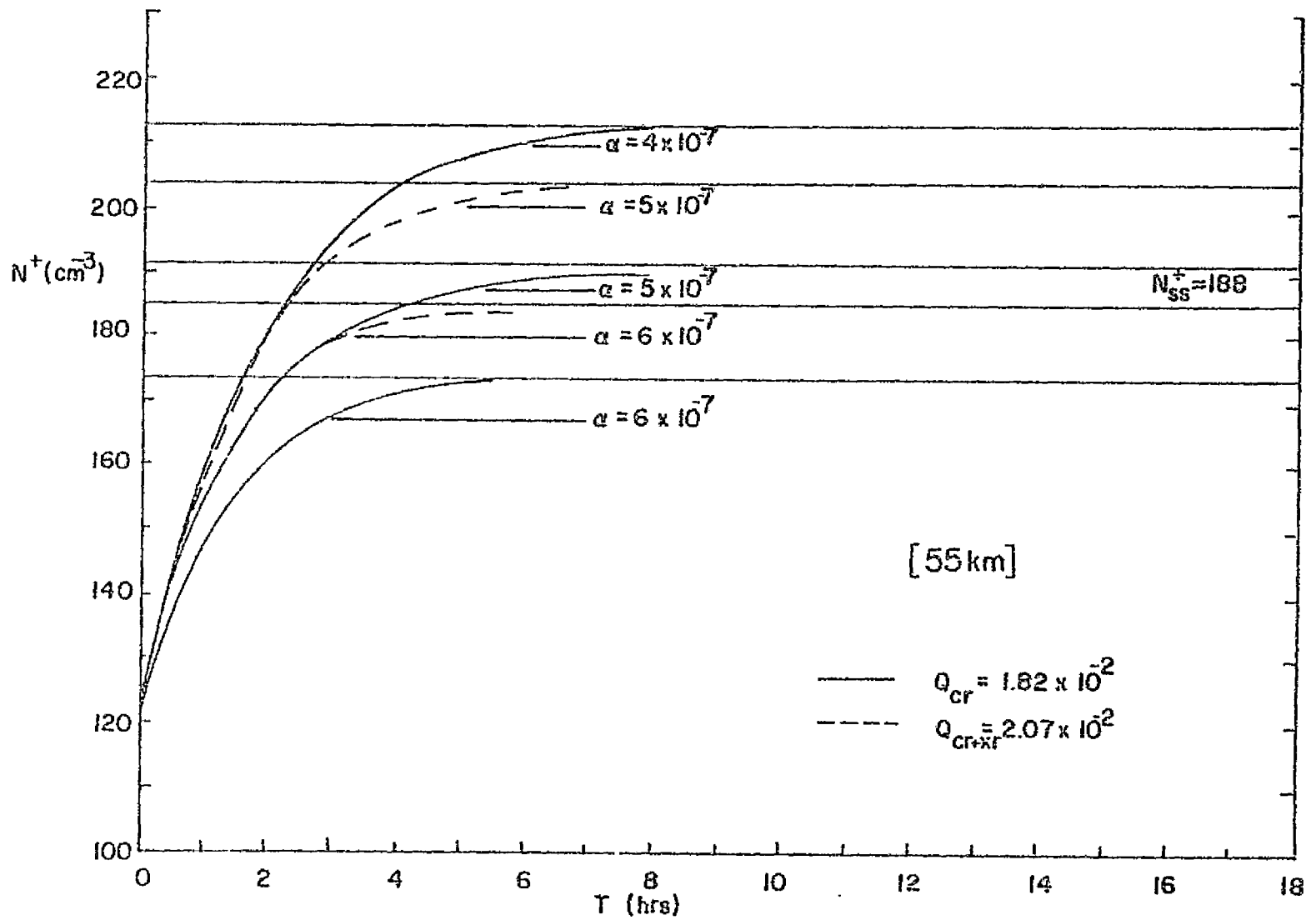
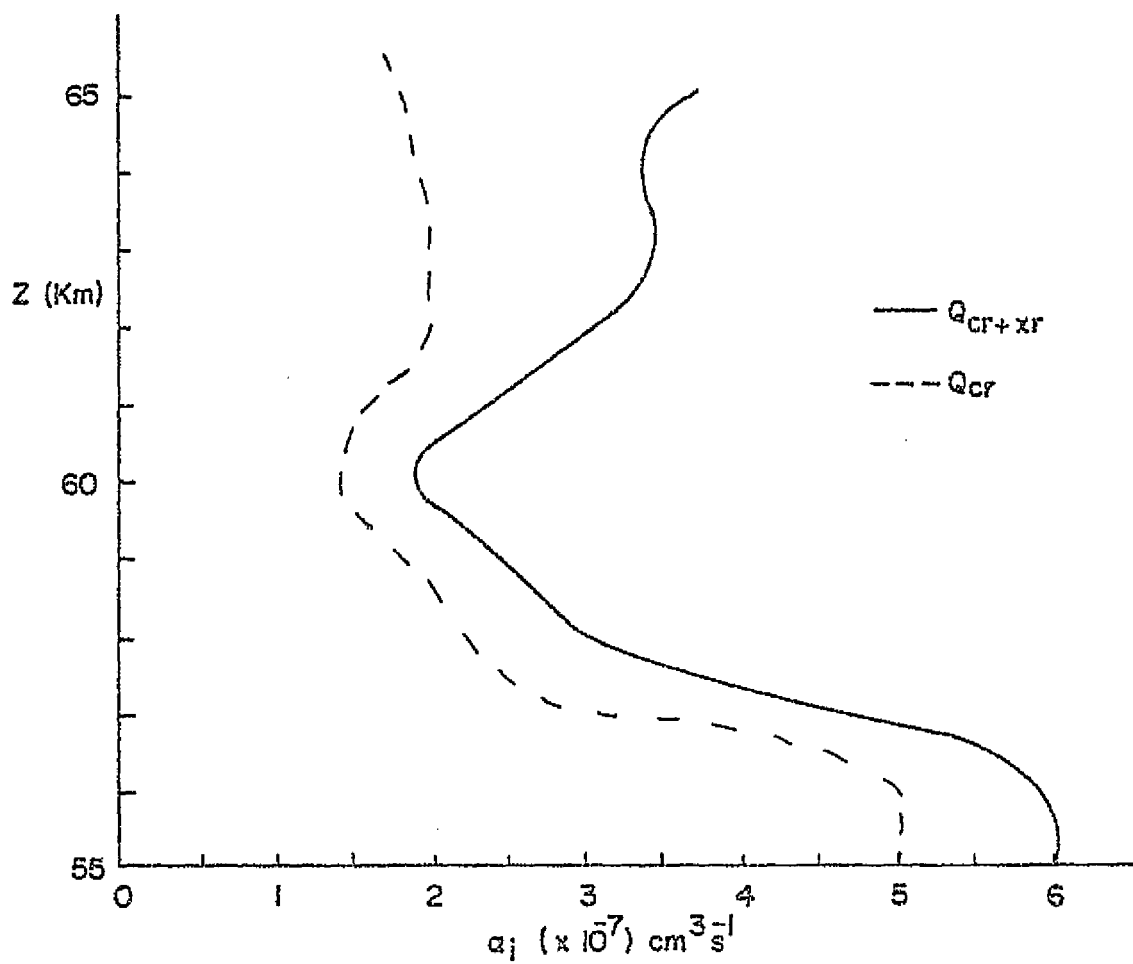


Figure 4.12 N^+ Versus Time at 55 Km

Figure 4.15 α_i 's Versus Altitude

ring. The fairly large scatter in α_i is due to the scatter in the Gerdien observed N^+ . The suppression of α_i from 61 to 59 Km results from an enhancement of N^+ in this layer (Figure 3.3) which may be an effect due to the temperature dependence of ion density (Cipriano, 1973) or of some unknown ionization source (see below). We will now present an argument for the latter explanation.

It is important to note, however, that the α_i of the cosmic ray + X-ray production calculations is in closer agreement to the ion-ion recombination coefficient as given by the DNA Handbook (1972). This value, $3 \times 10^{-7} \text{cm}^3 \text{s}^{-1}$ is almost equal to the average value of α_i in the 65-58 Km range, $3.1 \times 10^{-7} \text{cm}^3 \text{s}^{-1}$. The average value for the cosmic ray only production late calculations is below $2 \times 10^{-7} \text{cm}^3 \text{s}^{-1}$.

It appears that the cosmic ray + X-ray production model is more consistent with the accepted and standard values of two body ion chemistry reaction rates.

This conclusion is not totally surprising because during this rocket campaign, X-rays were measured at these levels and found to be comparable to calculated cosmic rays as ionization sources. Further, the observation made in Section 3.2, showing that the vertical extent of nighttime enhancement is coincident with the layer of maximum ion production due to X-rays, supports the conclusion.

This study indicates that the presence of X-rays should be considered as an important source of ionization in the lower D-region and that some of the observed radio wave effects attributed to transient celestial X-ray sources can be verified theoretically.

4.5 A Constant Recombination Coefficient Assumption

Previous measurements suggest that the ion-ion recombination coefficient, α_i , is constant with height between 55-70 Km (Hale, 1976). Therefore, equation (4.4) was employed again; this time α_i was held constant and Q was varied to obtain the proper, observed, steady state positive ion density. Figure 4.14 is a height profile of additional ion production, $\Delta Q (= (\alpha_i N^2) - Q_{\text{cos ray}} + \text{X-ray})$, that is required to explain the nighttime enhancements if one assumes α_i to be a constant. Three values of α_i were assumed; 4, 5, and $6 \times 10^{-7} \text{cm}^3 \text{s}^{-1}$. It is evident from the figure that under this assumption, a large ($\sim 1.5 \times Q_{\text{cos ray}} + \text{X-ray}$), sharply peaked at 60 Km, additional layer of ionization production is needed to explain the "Antarqui" data. The possible physical significance of this calculation remains unknown at this time and has not been explored further in this research.

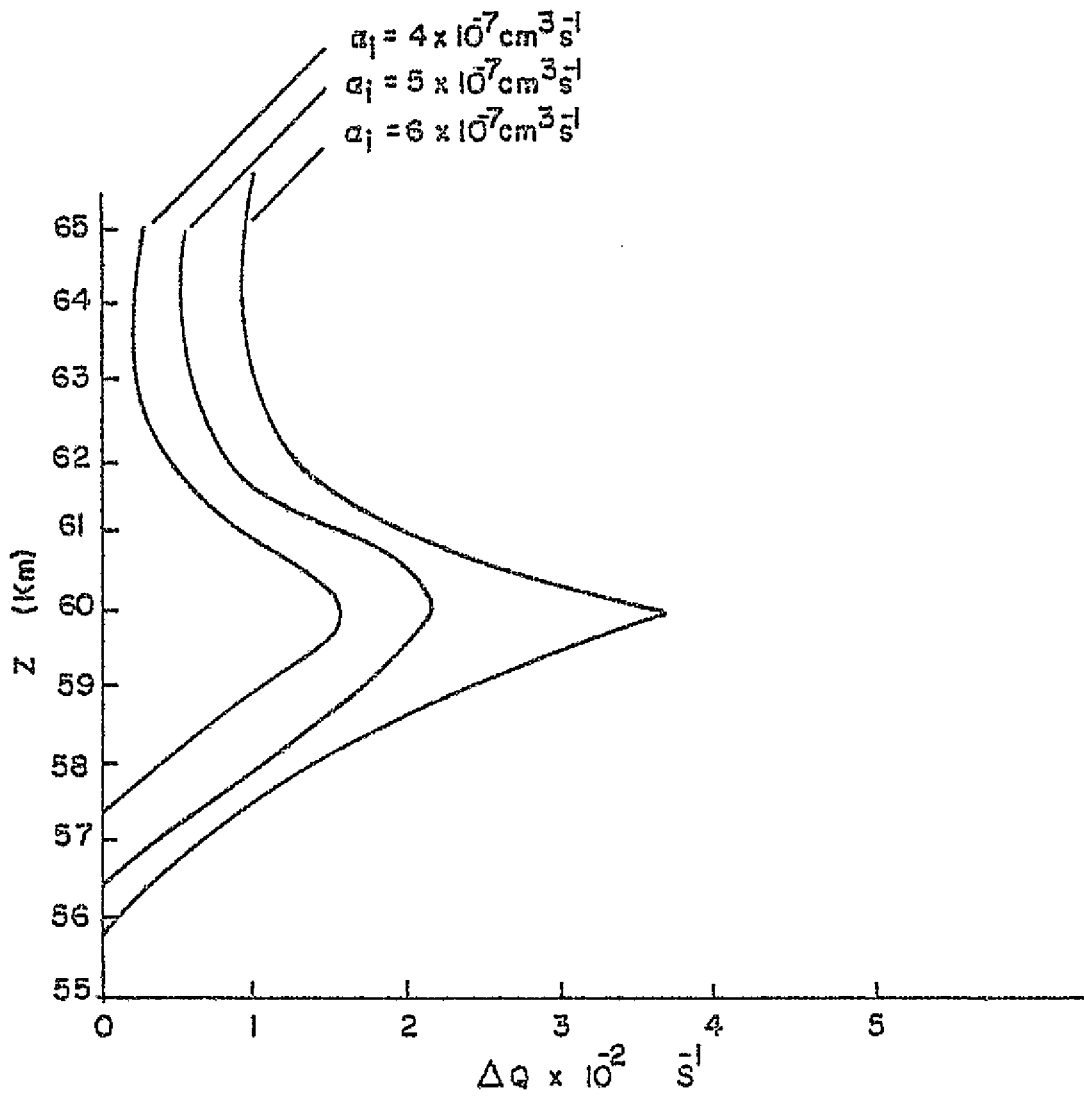


Figure 4.14 Additional Production Needed
If Constant α_i is Assumed

CHAPTER V

CONCLUSIONS

The ionization of the low latitude middle atmosphere has been investigated by the coordinated D-region "Antarqui" experiment, 23-28 May, 1975, Peru. Using data obtained during this campaign by The Pennsylvania State University Ionosphere Research Laboratory rocket launched parachute borne blunt probe and Gerdien condenser conductivity measuring devices, the present study concludes that:

(1) The relative constancy of positive conductivity between 65-50 Km indicates that this parameter is not strongly dependent upon atmospheric density. This conclusion has been stated by others using mid-latitude conductivity data (Mitchell, 1973).

(2) The "knee" or minimum of the day, evening, and night conductivity curves occurs at about 65 Km; this is the same altitude that the "knee" appears on mid-latitude data (Hale, 1973).

(3) Low latitude conductivities (and ion densities) are lower than those at mid-latitudes.

(4) Positive ion densities calculated by assuming a reduced mobility and observed blunt probe conductivities indicate that in the 65-50 Km layer they are approximately proportional to air density. This indicates a large number of electrons with roughly constant density, satisfying

a steady state, lumped ion continuity equation (Hale, 1973).

(5) The region of enhancement coincides very well with the altitudes where the ion production due to celestial X-ray sources are assumed to be on the order of other ionization sources. If this enhancement was merely a return to steady state nighttime equilibrium conditions, the affected layer would be significantly thicker, perhaps down to 40 Km, than the 50-70 Km region of observed enhancement (Hale, 1976).

(6) The observed day to night variations of positive conductivity indicated that, with conclusion (5) above, cosmic ray ionization below 65 Km is at least necessary to account for these variations. Further, theoretical calculations indicate that an additional source of ionization, due to X-rays, is significant (i.e. comparable to cosmic ray ionization) in the 65 ± 3 Km height range, if one assumes an ion-ion recombination coefficient of $3 \times 10^{-7} \text{cm}^3 \text{s}^{-1}$. This conclusion possibly is related to some of the reported changes in phase of VLF radio waves by transient, celestial X-ray sources. These individual sources contribute significantly to the total X-ray flux.

(7) If one assumes α_1 (ion-ion recombination coefficient) is constant in the height range 55-70 Km, an additional, large, sharply peaked at 60 Km, ionization layer is required to explain the "Antarqui" observations.

REFERENCES

- Ananthakrishnan, S., and K. R. Ramanathan, Effect on the lower ionosphere of x-rays from Sco XR-1, Nature, 233, 488, 1969.
- Barcus, J., Private Communication, 1975.
- Chilton, C. J., and J. H. Crary, VLF observations of nighttime D-region ionization enhancement by the Scorpius XR-1 x-ray source, Radio Sci, 6, 699-708, 1967.
- Cipriano, J. P., M. S. Thesis in Meteorology, The Pennsylvania State University, 1973.
- CIRA, Cospar International Reference Atmosphere, DNA Handbook, 1972.
- Clark, J. H. E., Private Communication, 1976.
- DNA, DNA Reaction Rate Handbook, 1972.
- Farrokh, H., Design of a simple Gerdien condenser for ionospheric D-region charged particle density and mobility measurements, Scientific Report No. 433, Ionosphere Research Laboratory, The Pennsylvania State University, University Park, Pennsylvania, 1975.
- Goldberg, R. H., Private Communication, 1975.
- Hale, L. C., Parameters of the low ionosphere at night deduced from parachute borne blunt probe measurements, Space Research VII, North Holland, Amsterdam, 140-151, 1967.
- Hale, L. C., Private Communication, 1976.
- Holton, J. R., Dynamics of the Stratosphere and Mesosphere, Meteo. Monographs, Vol. 15, No. 37, American Meteorological Society, Boston, 1975.
- Hoult, D. P., D-region probe theory, J. Geophys Res, 70, 3183-3187, 1965.
- Leiden, S. C., Private Communication, 1976.

- Loeb, L. B., Basic Processes of Gaseous Electronics, University of California Press, Berkeley and Los Angeles, 1961.
- Mitchell, J. D., An experimental investigation of mesospheric ionization, Scientific Report No. 416, Ionosphere Research Laboratory, The Pennsylvania State University, University Park, Pennsylvania, 1973.
- Mitchell, J. D., Private Communication, 1975.
- Mitra, A. P., and Y. V. Ramanamurty, Ionization contribution by cosmic x-rays, Radio Sci, 7, 67-72, 1967.
- Nawrocki, P. J., and R. Papa, Atmospheric Processes, GCA Corporation, Bedford, 1961.
- Nicolet, M., and A. C. Aikin, The formation of the D-region of the ionosphere, J. Geophys. Res., 65, 1469, 1960.
- Poppoff, I. G., and R. C. Whitten, Ionospheric effect of x-rays from Scorpius XR-1, Nature, 224, 1167, 1969.
- Potemra, T. A., and A. J. Zmuda, Precipitating energetic electrons as an ionization source in the mid-latitude nighttime D-region, J. Geophys. Res., 75, 7161-7167, 1970.
- Rishbeth, H. and O. K. Garriot, Introduction to Ionospheric Physics, Academic Press, New York, 1965.
- Rowe, J. N., Model studies of the lower ionosphere, Scientific Report No. 406, Ionosphere Research Laboratory, The Pennsylvania State University, University Park, Pennsylvania, 1972.
- Sharma, D. P., et. al., Possibility of continuous monitoring of celestial x-ray sources through their ionization effects in the nocturnal D-region ionosphere, Astrophys. Sp. Sci., 17, 409-425, 1972.
- Sonin, A. A., Theory of ion collection by a supersonic atmospheric sounding rocket, J. Geophys. Res., 72, 4547, 1967.
- Velinov, P., On ionization in the ionospheric D-region by galactic cosmic rays, J. Atmospheric Terrest. Phys., 50, 1891-1905, 1968.
- Whitten, R. C., and I. G. Poppoff, Fundamentals of Aeronomy, Doubleday, New York, 1971.

APPENDIX A
PROGRAM TO CALCULATE CONDUCTIVITIES

```

0:
PRT "PROGRAM TO
CAL-", "CULATE CO
DUCTI-", "VITIES
FOR BLUNT", "PRO
BES"
1:
ENT "XMIN", R0, "X
MAX", R1, "YMIN", R
2: "YMAX", R3
2:
SCL R0, R1, R2, R3
3:
ENT "ROUT", R0, "R
IN", R1, "RCAL", R2
, "SCL", R4, "REFAN
G", R5; 2.54/R3
4:
ENT "NOCAL", R6, "
NO DATD", R7; R0/2R
1R1R2R3/A; PRT "R
OUT=", R0, "RIN=",
R1
5:
IF R0<0; GTO 8
6:
PRT "RCAL=", R2, "
REFANG=", R5; SPC
5; 1+B; 9+C

```

```

7:
ENT "SLOPE", X;
TAN (R5+(INT X+(
X-INT X)/.61))+Y;
Y+C/C; 1+B+B; IF B
<R6; GTO +0
8:
PRT "AVRG CALSLO
PE=", C/R6, "LAST
SLOPE=", Y; SPC 2;
8+B
9:
ENT "SLOPE", X, "A
LT", R6; R6/R4+R6
10:
IF X<1; GTO 13
11:
TAN (R5+(INT X+(
X-INT X)/.61))+Y;
YAR6/C+R(B+R7)
12:
GTO 14
13:
X+R(B+R7)
14:
PLT LOG R(B+R7),
RB; PEN F
15:
PRT "ALT(KM)=", R
B, "SIGMA=", R(B+R
7); 1+B+B; IF B<R7
; GTO -6; SPC 2
16:
PRT "END OF THIS
GREAT FUN"; STP
/END F
P322

```

APPENDIX B
PROGRAM TO CALCULATE N^+
VERSUS TIME CURVES

```

0:
PRT "ASN VS T"
1:
ENT "XMIN",R0,"X
MAX",R1,"YMIN",R
2,"YMAX",R3
2:
SCL R0,R1,R2,R3
3:
ENT "Q",R0,"ALP"
,R1,"N0",R2
4:
1/R(R0R1)+R3
5:
R(R1/R0)+R4
6:
ENT "N",R5
7:
R5R4+R6
8:
R2R4+R8
9:
IF R6<1;GTO 13
10:
R(R0/R1)+R10
11:
PRT "ASYN",R10
12:
GTO 3
13:
R3*.5(LN ((1+R6)
/(1-R6))-LN ((1+
R8)/(1-R8)))+R9
14:
R9/3600+R9
15:
PRT "TIME",R9,"N
UM",R5
16:
PLT R9,R5
17:
R5+5+R5
18:
GTO 7
19:
END
R362

```